Check for updates

Hydration-induced reversible deformation of biological materials

Haocheng Quan [ID][1], *David Kisailus* [ID][2] *and Marc André Meyers* [ID][1] ✉

Abstract | The influx and efflux of water in biological structures actuates reversible deformation and recovery processes that are crucial for mechanical functions in plants and animals. These processes utilize various mechanochemical mechanisms: swelling directed by the arrangement of cellulosic microfibrils in a bilayer construct, which generates different deformation patterns; lignification gradients; hierarchical foam-like inner structures, some of which also include swelling by hygroscopic cellulose inner cell layer; turgor pressure, which is activated by osmosis and acts at the cellular level, generating reversible motions. In this Review, we present representatives of each of these four mechanisms: pine cones, wheat awns, the twisted opening of *Bauhinia* pods and the seed of the stork's bill; the resurrection plant; ice plant seed capsules and carrotwood seed pod; the wilting and redressing of plant stems. Natural polymeric materials produced by animals can also exhibit hydration-driven shape and strength recovery: bird feathers and hair are prime examples. Spider silk — a non-keratinous biopolymer — also exhibits humidity-driven reversible deformation. After describing these animal-based mechanisms, we outline bioinspired applications to actuate multifunctional and biocompatible smart materials, and indicate future directions of research with potential for new bioinspired designs.

With the increasing complexity of systems, integration of materials into intelligent devices (for example, robots, self-driving vehicles, portable health monitors and personal assistive devices)[1,2] that can respond in an appropriate manner to the external stimuli without interference presents many scientific and technical challenges. To address this, programmes such as the Materials Genome Initiative[3] are providing opportunities to conceive new functional materials. Concurrently, machine learning, which is a rapidly developing research area that relies on big data and, as such, is a branch of artificial intelligence, offers potential to accelerate the design of novel materials with higher efficiency[4–6]. The combination of these programmes is providing, in part, the impetus to develop a range of smart materials, such as those for self-diagnosis[7,8], self-degradation[9,10], self-repair or healing[11–13], self-colouring[14,15] and self-shaping or morphing[16–18]. Among these categories, the most widely investigated are self-shaping materials (also called shape-memory materials), which have the ability to change, or even program in some cases, their shape or morphology based on external stimuli.

A wide range of self-shaping materials have been fabricated, including assorted alloys[19], polymers[20], ceramics[21] and composites[22]. The triggers to induce these predesigned morphologies include heat, light, electricity, magnetic fields, moisture or solvents. These synthetic, smart, self-shaping materials have important roles in applications, such as actuating robotic systems[23,24], camouflaging armour[25], biomedical devices[26,27] and drug delivery[28,29]. Nevertheless, one major stumbling block to the development of self-shaping materials, especially with respect to application within the human body, is their biocompatibility: either the material composition of these structures is toxic or their triggering and operating environments (for example, high temperature, electromagnetic fields and solvents) are harmful to our health. To circumvent the aforementioned challenges, researchers are looking at natural systems to inspire their quest for biocompatible self-shaping materials (as well as other smart materials) that can be stimulated and operated in mild environments.

Nature ingeniously develops efficient structural and functional materials, which manifest fascinating properties that are often superior to their synthetic counterparts[30–32]. Driven by hundreds of millions of years of evolution, numerous self-tunable materials that are crucial to the survival in various environments have been identified. Some material systems are considered active, in that the responsiveness of the tunable property relies on the metabolism of the living organism. For example, chameleons[33] and some species of squid[34] can actively modulate their skin colour and texture to camouflage themselves. Echinoderms, like sea

[1]*Materials Science and Engineering Program, University of California, San Diego, San Diego, CA, USA.*

[2]*Department of Materials Science and Engineering, University of California, Irvine, Irvine, CA, USA.*

✉*e-mail: mameyers@ eng.ucsd.edu*

cucumbers, can reversibly modify the stiffness of their dermis by rapidly regulating the interaction between the collagen fibrils and the soft reinforcing matrix, which plays an important role in complex locomotion, postural maintenance, defence and reproductive strategies[35,36]. Plants have also evolved strategies to actively respond to external stimuli, benefiting their survival. Two representatives are mimosa[37] and the Venus flytrap[38], both of which can achieve expeditious reversible deformation of their leaves and are triggered by the loss of turgor in their cells. These stress responses are vital to their self-defence or predation.

Another class of responsive natural materials that is generating interest in the materials-science and structural-engineering communities is plant organs and animal tissues that display passive stimulation. In such materials, there is no metabolism or muscle work involved in the actuation process and, thus, the tissues are not living. An example of passive stimulation is the reversible shape change triggered by changes in moisture content, which is a prevailing strategy for plants to disperse their seeds. Pine cones, ice plant seed capsules, carrotwood seed pods and some pea pods can release their seeds in favourable environments by actuating structures driven by humidity change[39–41]. The seeds of wild wheat and the stork's bill (*Erodium cicutarium*) can bury themselves in soil through reversible hygroscopic bending or coiling, which significantly increase their survivability[42,43]. Some biological materials produced by animals have a similar capability. Keratinous-based structures, such as bird feathers, sheep horns and animal hairs, are able to recover their shape and retain mechanical properties — mainly strength — through hydration effects[44–47]. Spider silk is an excellent example of a natural biopolymer displaying highly reversible supercontraction stimulated by humidity change[48,49]. The underlying deformation mechanisms of these processes are determined by the material and structural design, an understanding of which could inspire the development of novel responsive materials.

In this Review, we provide an interdisciplinary perspective, incorporating materials science, structural engineering and biology, highlighting well-known examples of highly reversible deformation in natural systems. Although we focus on plant organs, some animal tissues will also be discussed. Most of the reviewed structures display purely passive deformation, which relies on their hierarchical structural design and hydration-driven actuation. We present three passive hydro-actuation mechanisms for the selected plant samples and one general recovery mechanism for animal tissues. We also briefly review the active mechanism by which live plants exhibit either flaccid or erect configurations, based on changes in internal pressure (that is, turgor) inside of the cells. We describe smart materials inspired by these biological materials, including multiscale self-shaping materials and artificial muscle fibres that can generate impressive forces. Based on the systems provided in this Review, new designs and strategies are discussed for the development of smart responsive materials that have desirable mechanical properties and biocompatibility.

Mechanisms of plant movement

Plants produce a large variety of multifunctional biological materials to ensure survival. Although they are not nearly as mobile as animals, if we observe their activities via time lapse, their life is equally vivid and lively. Skotheim and Mahadevan[50] summarized typical movements in plants and fungi, providing a brief but insightful perspective on their physical basis. Plant and fungal movements can be classified based on the smallest dimension (from micrometres to metres) and timescale (from microseconds to days) of the moving unit. The absolute speed limit for all movements is determined by the speed of the elastic waves in the plant organs. All actuating plant movements are slower than this speed limit and are divided into two groups: those based on mechanical instability and those based on diffusion.

Movements based on mechanical instability are significantly faster than diffusion-based ones and are achieved by elastic instabilities. In some species, these movements are dominated by a snap-buckling instability. The best-known example of this is the rapid closure of the Venus flytrap[51], which can capture its prey (that is, insects) within 0.1 s. A similar mechanism is found in the *Aldrovanda*, the snapping speed of which is even faster, owing to its thinner leaf (than that of the Venus flytrap). Another type of fast movement is enabled by explosive fracture seen in species such as *Cardamine hirsuta*[52], *Polypodium aureum*[53] and *E. cicutarium*[54]. In these cases, the elastic energy stored in extremely deformed organs is suddenly released when its tissue is fractured owing to dehydration[55,56], providing a large amount of kinetic energy to disperse the seeds with an impressive initial speed ($\sim 10\,\mathrm{m\,s^{-1}}$)(REF.[52]).

In the class of diffusion-based actuation, movement is generated by swelling or shrinking of plant organs due to differential hydration. Because such movements are limited by fluid transport, they are usually relatively slow and undetectable to the human eye. Nonetheless, they are vital for plant growth, prey and sunlight capture, seed dispersal and self-defence. Three well-known examples, which will be discussed later, are the pine cone[39], ice plant seed capsule[40] and resurrection plant[57]. They can actuate their characteristic structures by hydration, which has an important role in their seed dispersal and self-protection in different environments. In contrast with movements relying on elastic instability, hydro-actuated anisotropic swelling and shrinking is purely passive and highly reversible[58]. These attributes may provide value to materials scientists for the development of robust self-shaping materials. These mechanisms are, for the most part, based on bilayer constructs in which the differences in contraction and expansion between the two layers lead to a variety of deformation patterns. Consequently, they are also the main focus in this Review.

Anisotropic swelling of microfibrils

Cell structures and actuation mechanisms. The morphology and functionality of plant cells are distinct from those of animal cells: they have a cell wall and an extracellular structural material that acts as a supportive framework and provides mechanical stability to the cell, maintaining turgor pressure and protecting inner
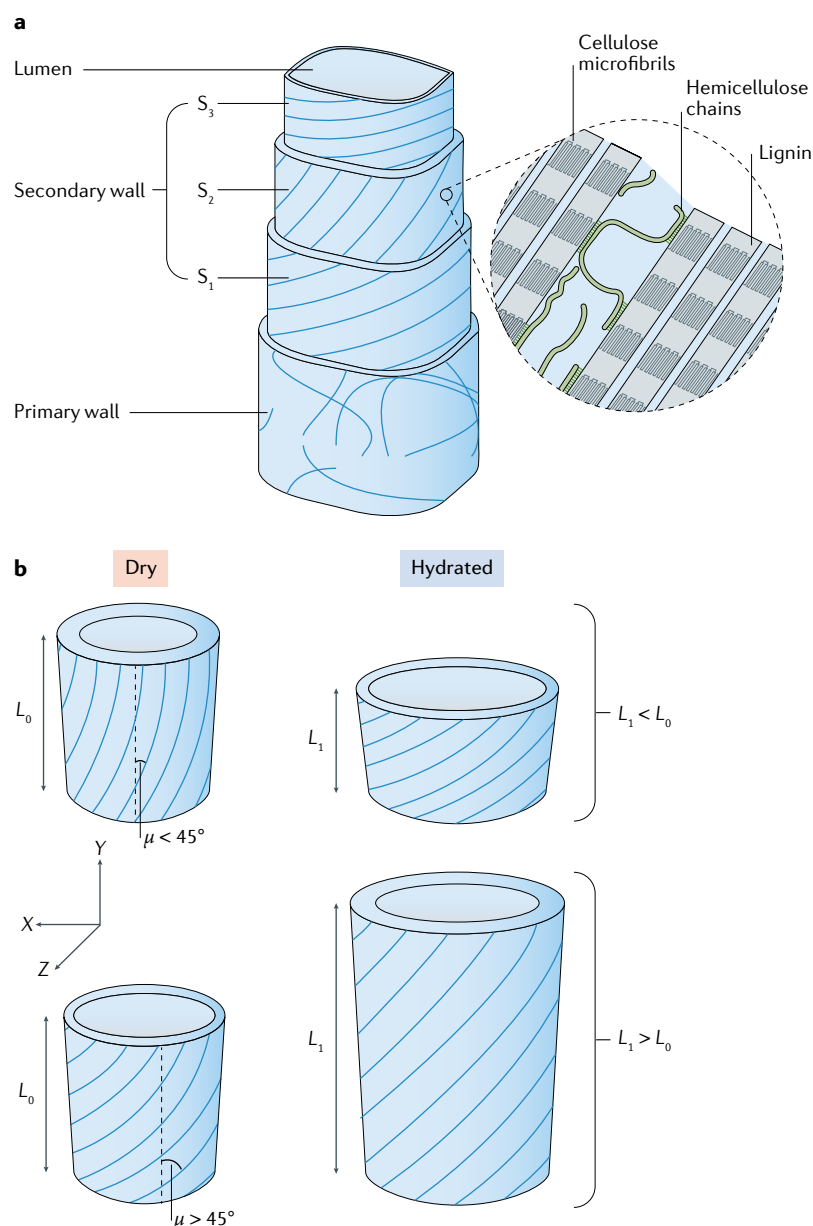
Fig. 1 | **Mechanisms of hydration-induced movement. a** | Schematic hierarchical structure of the secondary cell wall in a wood fibre cell[60]. Each cell wall is composed of the primary wall and the secondary wall, with the latter consisting of three layers: S_1, S_2 and S_3. The layer S_2 is the major component and is the thickest. The orientation of the cellulose microfibrils in these three layers is twisted to form a helical structure, and the centre of the cell is the hollow lumen. The cellulose microfibrils in the secondary wall are embedded in a matrix that is composed of hemicellulose and lignin, which function as crosslinks and fill the interfibrillar spaces. Cellulose microfibrils are composed of cellulose chains, which are partially crystallized and stiffer than hemicellulose and lignin. **b** | Schematic of the S_2 layer — the major component of the secondary cell wall in plant cells — which has stiff cellulose microfibrils embedded in a swellable matrix[59]. L_0 is the original length and L_1 is the deformed length. The microfibril angle, μ, is the angle of the direction of twist of the cellulose microfibril with respect to the longitudinal axis of the cell (Y-axis). The dimensional changes depend on the size of μ: for $\mu \leq 45°$, shrinking occurs, and for $\mu \geq 45°$, extension occurs. Panel **a** is adapted from REF.[60], Springer Nature Limited.

organelles. The plant organs or tissues deform owing to the restriction of the internal stress generated by the expansion and shrinkage of their thick, rigid cell walls, even in dead cells[59]. However, the walls of living and

dead cells are different. Once the cells are fully mature and dead, they become structural extracellular materials; the organelles of plant cells and the plasma membrane disintegrate, and the centre of the cell forms a hollow lumen[60] (FIG. 1a). The outermost layer of these cells is the primary wall, which consists of randomly oriented cellulosic microfibrils. The major component of wood fibre is the secondary cell wall, which has three layers (denoted by S_1, S_2 and S_3). Each consists of a specific array of cellulosic microfibrils embedded in a compliant and amorphous matrix, composed of lignin and hemicellulose. The cellulose microfibrils are assembled by several interconnected cellulose molecular chains that form alternating crystalline and amorphous phases[61,62]. As a consequence of their crystallinity, the cellulose microfibrils are much stiffer than their surrounding matrix. Thus, the mechanical properties of the entire wood cell wall are dominated by the arrangement of the cellulose microfibrils. The orientation of cellulose microfibrils within each layer is unidirectional, but the orientation differs from layer to layer. In most cases, because S_2 is the thickest layer in the secondary cell wall, the mechanical properties of the entire cell wall are dominated by the arrangement of its cellulose microfibrils. There are also some cases that the swelling and shrinking is caused by the G-layer inside of the plant cell wall[63,64], but the swelling strain mismatch is also due to the microfibril arrangement.

The Fratzl–Elbaum–Burgert model[59] quantitatively connects the hydroelasticity of the plant cell wall and the orientation of its cellulose microfibrils. This model describes a thin-walled hollow cylinder (FIG. 1b). The angle between the microfibril orientation and the cell wall axis is defined as the microfibril angle and is denoted by μ. The matrix, in which the cellulose microfibrils are embedded, is assumed to bear elastic swelling isotropically with increasing humidity. This mechanism is analogous to that for the shape recovery for keratin[43]. In the case of microfibrils, the amorphous phase absorbs the humidity and swells, whereas the crystalline filaments remain unchanged. Furthermore, the model assumes that the swelling strain remains uniform in the X–Y plane and that there is no torsion of the cylinder because it is confined within a thick tissue, which makes it a plain-strain condition. The fibrils' relative modulus is the ratio between the Young's modulus of cellulose microfibrils and that of the matrix, namely, $(1 - v^2)E_F/E$, where E_F, E and v are the Young's moduli of the fibrils and matrix, and the Poisson coefficient, respectively.

This model yields three important implications. First, when the microfibril angle is small ($\mu < 45°$), the stiff cellulose microfibrils can restrain the swelling and the cell wall resists expansion along the longitudinal axis; however, the hydrated cell wall expands radially as the longitudinal dimension shrinks (FIG. 1b). Second, when the microfibril angle is large ($45° < \mu < 90°$), the restraining effect of the stiff fibrils is reduced. As a result, the cell wall is freer to swell along its longitudinal axis, the hydrated cell wall expands longitudinally and the radial dimension shrinks (FIG. 1b). Third, with larger relative moduli of fibrils, this anisotropic swelling effect is more

obvious. Thus, the model[59] provides mechanistic insight into the origin of anisotropic swelling in plant tissues.

By manipulating structures through anisotropy, nature creates intricate hygroscopic movements, like bending, twisting and coiling (also called helical twisting). In the following section, we provide examples of the actuation mechanisms that generate such movements. From a biomimetic viewpoint, these mechanisms provide inspiration for complex actuation that might be achieved by reinforcing compliant gels with stiff nanofibrils or nanotubes.

Bending, twisting and coiling movements

The most common humidity-driven reversible movements in plants are actuated based on the anisotropic swelling caused by varied microfibril angle. In this section, we introduce three types of movements — bending, twisting and coiling — and provide specific examples of each. All of these movements are important in seed dispersal and sowing.

Bending is the most common movement because it is easy to achieve, as long as there is a noticeable strain mismatch in a well-integrated bilayered structure[65]. A well-studied example is the pine cone[39,66–68] (FIG. 2a). Under dry conditions, dehydration drives the pine cone to open. The seeds are then released and carried by wind over long distances. On rainy days, the cone is closed to protect the seeds from escaping; because, in this weather, the seeds would fall too close to the parent plants and not germinate. This strategy of seed release and protection is achieved through the reversible bending deformation of the cone scales. The scales of the cone bend outward with the reduction of hydration to release the seeds. A network of diverging fibres is revealed inside the scale (Supplementary Fig. 1a, Supporting Information). A polished longitudinal section of a cone and an isolated scale reveal the bilayered structure of the scale: the upper part is thinner but much brighter (called sclerenchyma fibres) and the lower part is darker and is composed of sclereids. Scanning electron microscopy images of the cell wall for these two parts[37] (right panels in FIG. 2a) show that the cellulose microfibrils are almost parallel to the longitudinal axis in the upper part (sclerenchyma fibres), resulting in a low microfibril angle (μ ~30°). This alignment restrains the hygroscopic swelling in the fibre direction. By contrast, the sclereid-containing tissue in the lower part has a much higher microfibril angle (μ ~74°), leading to a free swelling of this region upon an increase in humidity. The different swelling responses for the two parts lead to the bending of the scale upon changes in humidity.

A similar principle of movement is identified in wild wheat awns[42,63,69]. The awns of wild wheat can bend and straighten, driven by the change of relative humidity (FIG. 2b). This bending is also produced by the heterogeneous architecture inside the stem of the awn. Scanning acoustic microscopy images (FIG. 2b) reveal two distinct compositional regions: the cap, which is brighter, and the ridge, which is darker. The corresponding wide-angle X-ray scattering pattern (FIG. 2b) indicates that the cellulose microfibrils in the cap region are laid almost parallel to the cell axis, restricting the swelling and shrinkage

along the cell axis; by contrast, the tissue in the ridge region has multilayered cell walls with randomly arranged microfibrils, which leads to more isotropic shrinkage and swelling of the tissue upon humidity changes. As a result, the difference in the swelling and shrinkage of the inner and outer parts of the awns results in a slow bending movement of the awns upon ambient humidity change. The cyclic changes between the relatively dry air during the day and higher humidity at night can lead to a slow crawling-like movement of the seed-dispersal unit, whereas small spike-like silica hairs on the outside of the awns ensure a progressive forward movement by preventing the unit from moving backwards and out of the soil (Supplementary Fig. 1b).

Twisting is another common, passive, hygroscopic movement, which is usually identified in the seed pods of some plants, such as the legume family Fabaceae[70]. For example, Bauhinia pods, which are also called chiral seed pods, open and close their seed pods using a twisting movement upon humidity change[41] (FIG. 2c). Each valve of the Bauhinia pod consists of two layers of stiff fibre cells oriented roughly at ±45° with respect to the pod's longitudinal axis (FIG. 2c), which causes the preferential swelling and shrinking directions. The presence of two layers that shrink in perpendicular directions is sufficient to generate the flat-to-helical transition observed during pod opening. To prove this mechanism, two planar latex sheets were stretched uniaxially along two perpendicular directions and then glued together, forming a residually stressed compound sheet (Supplementary Fig. 1c). The elongated strips cut out from the composite sheets were found to curl into helical configurations, confirming that the twisting movement of the pea pods is actuated by the mechanism proposed above[41].

In contrast with Bauhinia pods, which twist around the long axis of the unit, the stork's bill (E. gruinum) separates from its fruit by coiling its awn when it is fully mature and dehydrated. By the movement upon the humidity change in daily cycles, the awn can reversibly coil and uncoil[54] (FIG. 2d), providing a propulsion to help its seeds drill into the soil. Unlike the common elongated cells in which the cellulose fibrils are wound in a helix around the cell wall, the stork's bill awn has a tilted helical arrangement of cellulose microfibrils within the cell wall[41] (model in the right panel of FIG. 2d), resulting in a varied threading angle of the microfibril along the cell wall. A simplified mechanical analogue made with swellable sponges and stiff threads proves that the normal helical winding produces normal twisting, whereas the tilted helix can generate coiling[41] (Supplementary Fig. 1d), which directs the seed to a safe germination site.

Gradient lignification

There are additional examples of simple hygroscopic movements that are also caused by the anisotropic deformation of plant tissue, where the anisotropy is not based on the cellulose microfibril angle but, rather, on gradients in lignin within different regions of the plant cell wall. Such is the case of structures found in resurrection plants.

Resurrection plants, such as *Selaginella lepidophylla*, flourish in desert regions and have an extraordinary
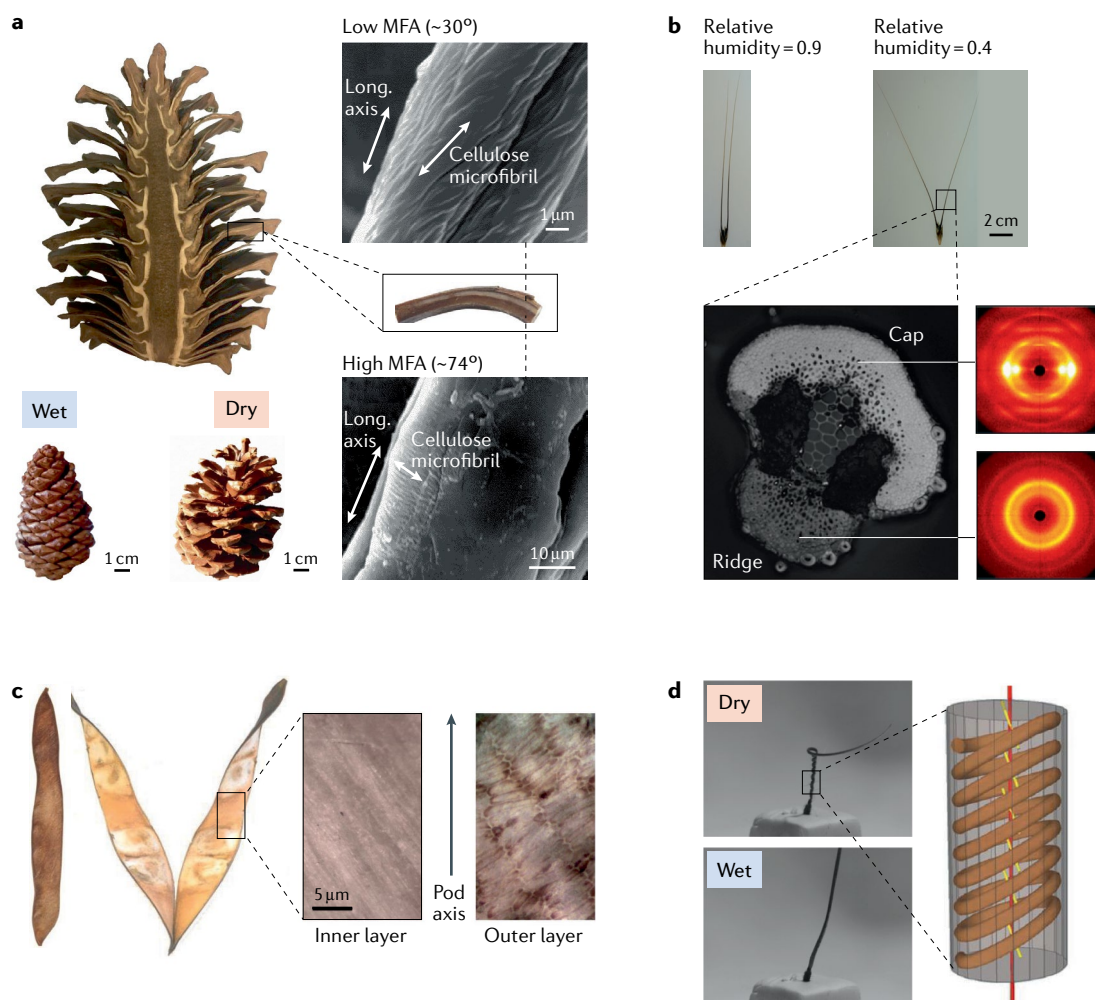
Fig. 2 | **Hygroscopic movements that enable plants to disperse or self-bury their seeds. a** | The bending movement of pine cone scales. The pine cone opens under dry conditions to release seeds and closes in wet state to protect seeds (left). A polished cross section shows a double-layered inner structure (right, middle). The light-coloured upper layer is composed of sclerenchyma fibres and the darker lower layer primarily consists of sclereids. Scanning electron microscopy images of cell walls in sclerenchyma fibres and sclereids are shown (right). The microfibril angle (MFA) between the longitudinal axis (labelled 'Long. axis') of sclerenchyma fibre and the direction of twisting of the cellulose microfibrils is equal to ~30°. In the sclereid layer, the MFA is ~74°. **b** | The bending movement of wild wheat awns driven by daily humidity changes. The scanning acoustic microscopy image shows the cross section of an awn stem, which is composed of two regions: the cap and the ridge (by 1×0.8 mm^2 field, brightness level is correlated to the relative impedance). The wide-angle X-ray scattering patterns of the crystalline cellulose at the cap and the ridge are shown (right). **c** | The twisting movement of the pod opening in *Bauhinia variegate*. The flat valves of the closed pod curl into helical strips when they are open in a dry state. Images of the inner layer (sclerenchymatous stratum) and the outer layer of the pod valve show that the cells are oriented ~45° to the pod axis but are perpendicular to each other. **d** | The hygroscopic coiling in a stork's bill awn. Passive hygroscopic coiling and uncoiling movements of the awn are induced by the absorption and loss of water. The schematic drawing shows the tilted arrangement of cellulose microfibrils on the coiling cell wall of the awn. Scanning electron microscopy images in Panel **a** are adapted from REF.[39], Springer Nature Limited. Panel **b** is reprinted with permission from REF.[42], American Association for the Advancement of Science. Panel **c** is adapted with permission from REF.[41], American Association for the Advancement of Science. Images in panel **d** are adapted with permission from REF.[54], The Company of Biologists. The drawing in panel **d** is republished with permission of The Royal Society of Publishing, from REF.[43], Tilted cellulose arrangement as a novel mechanism for hygroscopic coiling in the stork's bill awn. Abraham, Y. et al. **9**(69), 2012; permission conveyed through Copyright Clearance Center, Inc.

capability to resist desiccation[57]. Their branches contract with drying, curling the plant into a tight ball. Incredibly, they can hibernate for up to a century (FIG. 3a). After they curl, they can be transported large distances by the wind, rolling on the ground, travelling through deserts, even crossing continents[71]; this behaviour is similar to the tumbleweeds of the Western United States. Within

the curled plant, the inner green tissue remains attached and closed, protecting the fruits and seeds from being dispersed during extreme droughts. If there is a rare rainy event, the ball absorbs the water and uncurls itself within several hours (FIG. 3b), waking up the plant from its dormant state and causing the capsular fruits to open and disperse the seeds.
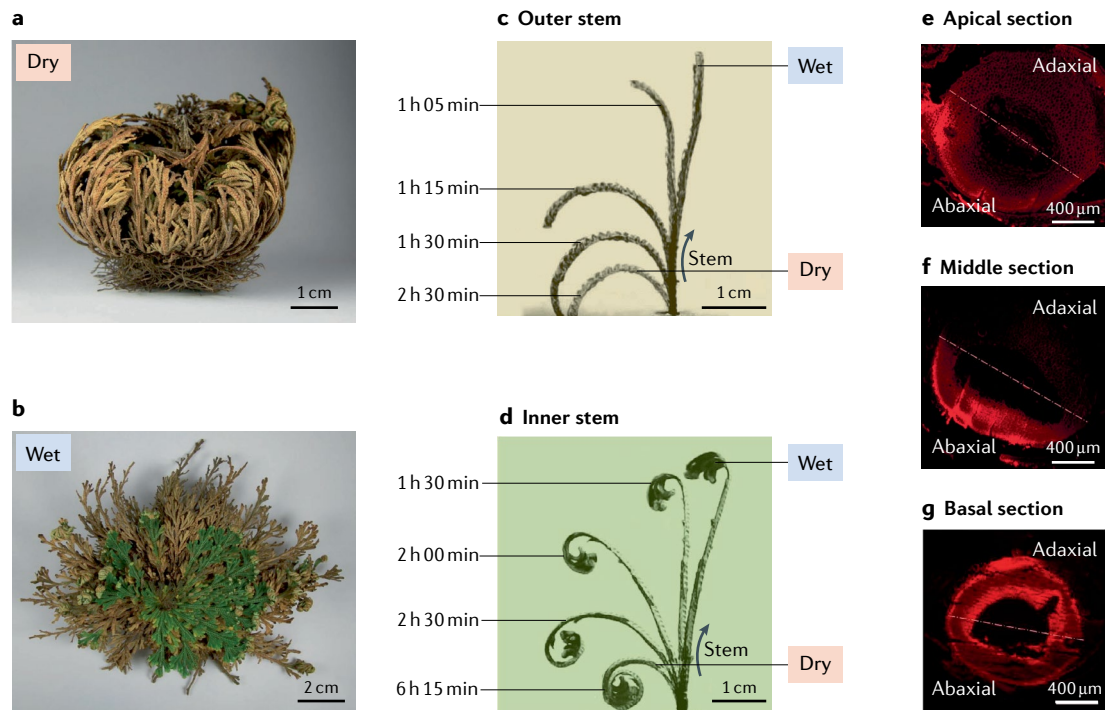
Fig. 3 | **Hygroscopic movements induced by gradient lignification in resurrection plant *Selaginella lepidophylla*.**
A resurrection plant (*Selaginella lepidophylla*) in dry (panel **a**) and wet (panel **b**) states. Its outer layer (panel **c**) contains older stems that curl with less curvature during the dehydration process than its inner-layer stems (panel **d**). The curved arrow indicates the opening direction of the stem. The cross sections of a stained inner-layer stem at the apical (tip) (panel **e**), the middle (panel **f**) and the basal (panel **g**) sections show a gradual change in lignification (bright red) from the stem base to the tip, and from the external (abaxial) side to the internal (adaxial) side. This cross-sectional variation in lignification enables the curvature to change on hydration. Reprinted from REF.[57], Springer Nature Limited.

FIGURE 3c,d depicts the curling process of an isolated stem from the outer and inner regions upon desiccation. The curling curvature of the outer stem is smaller than that of the inner stem, which allows the branches from different regions to coordinate to retract the plant into an integrated ball, providing optimal protection. This hydro-actuated process of curling and uncurling is reversible over several cycles. The ability of the plant to move in this manner is attributed to the presence of a lignin gradient within the stem tissue. Because the higher degree of lignification can increase the stiffness of the tissue and, consequently, reduce its ability to swell, the lignin gradient within the stem causes the branch to curl. FIGURE 3e–g shows the stained cross sections of an inner stem from the apical (top) region to the basal (bottom) section. The red stain indicates a profusion of lignin. Lignification on one half of the stem gradually decreases from the abaxial (outer) side to the adaxial (inner) side. Thus, the apical (top) part curls more than the basal part (bottom). This gradient generates the anisotropic swelling and shrinking of the plant branches and produces the highly reversible hydro-actuated deformation for the resurrection plants to protect themselves.

Hierarchical foam-like structure

Another prevailing type of hygroscopic material is enabled by foam-like structures, including cleaning sponges, such as the luffa (*Luffa aegyptiaca*)[72] (Supplementary Fig. 2a), which are used on a daily basis. The hydrophilic foam structure absorbs or loses water upon humidity change, resulting in a reversible change in the overall shape. The hierarchical foam structure (Supplementary Fig. 2b) consists of porous struts, confirming that the luffa sponge has a cellular structure at small length scales. Because of these attributes, luffa can be deformed and crushed, but, upon being hydrated, will regain its original shape, which will enable it to float, carrying the seeds away from their origin (Supplementary Fig. 2). Supplementary Fig. 2c shows the compressed luffa regaining its shape upon hydration. Deformation-generated, locally buckled and compressed struts are seen at the micrometre scale (Supplementary Fig. 2d). Because the plant tissue is highly hydrophilic, the deformed sponge can rapidly recover its original shape (in less than 10 min) (Supplementary Fig. 2e) by absorbing water to expand its cellular structure through the straightening of the struts (Supplementary Fig. 2f). This porous architecture serves as a dispersal medium.

Other hygroscopic biological systems actuated by a hydrophilic foam structure are found in the ice plant (*Delosperma nakurense*) seed capsule[38] and the carrot-wood (*Cupaniopsis anacardioides*) seed pods. The desert habitat of ice plants causes them to only release seeds in moist conditions, which may increase their chance of germinating in favourable environments. During their dormancy in a drought, the seeds are protected in compartments by five sealed valves in the capsule (FIG. 4a). As the surrounding moisture content increases, the active
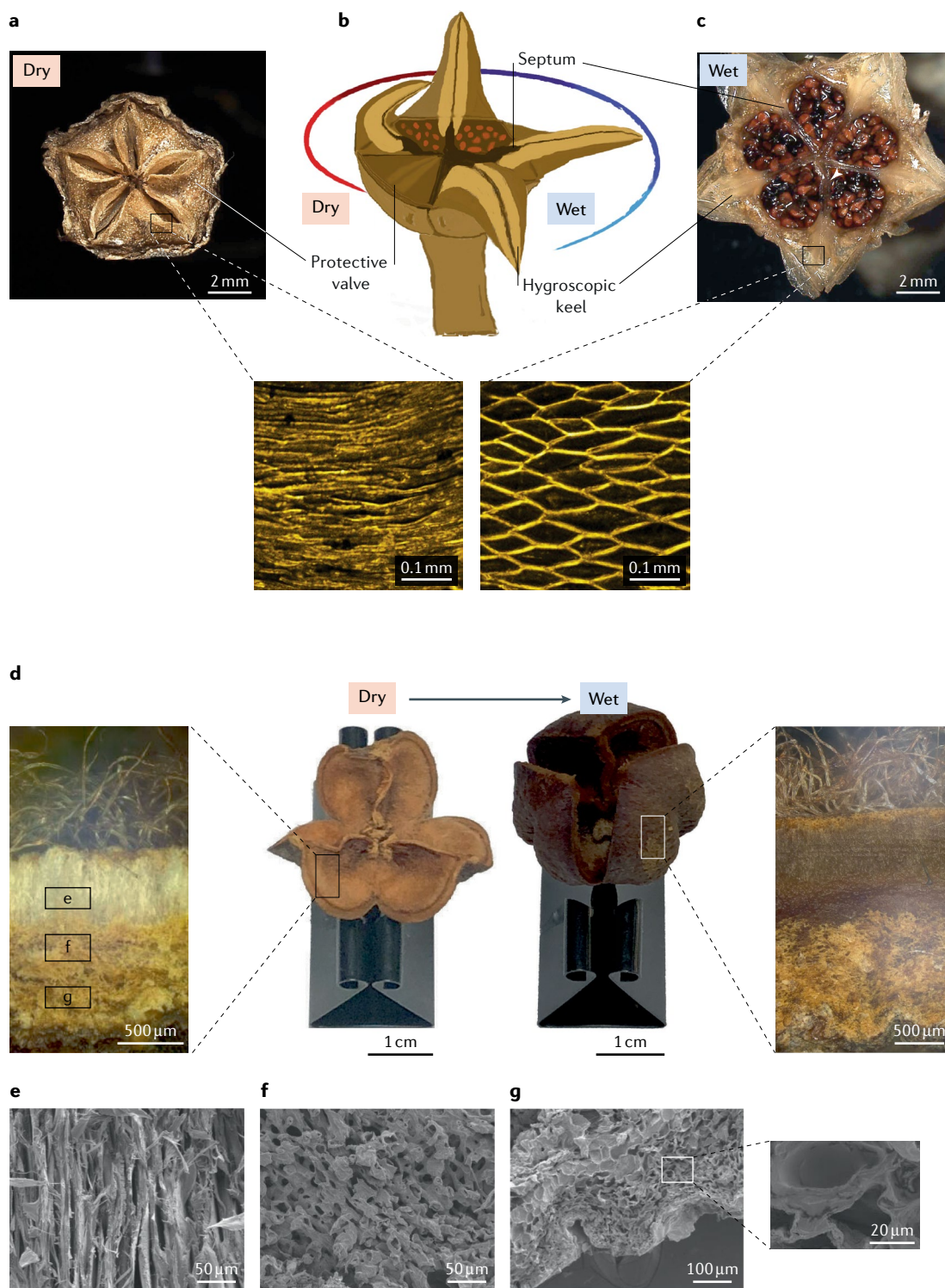
Fig. 4 | **Hygroscopic structure in an ice plant seed capsule and the porous structure in a carrotwood seed pod. a** | In a dry state, the ice plant seed capsule is closed and the cell wall is collapsed (as observed in the confocal microscopy image). **b** | Opening of a protective valve during hydration. **c** | In a wet state, the seed capsule opens and hydration-induced swelling of the cell wall in the upper layer occurs. The confocal microscopy image reveals that the hygroscopic keels have a honeycomb lattice structure with elliptical-shaped cells. This structure of the keel of the valve tissue causes deployment of the entire capsule. **d** | Hydration-induced opening and closing of the carrotwood (*Cupaniopsis anacardioides*) seed pod. The cross sections of the open (dry) and closed (wet) seed pod valve show the inhomogeneous swelling of the bilayer structure. The scanning electron microscopy images correspond to the three regions marked in the cross section of the dry state, which are shown in panels **e**, **f** and **g**. **e** | The top (inner) layer is composed of well-aligned fibres. **f,g** | The bottom (outer) layer has a porous structure made of the cell lumen (central cavity). The pore size gradually increases, forming a transitional region (panel **f**) to the bottom area (panel **g**). Panels **a–c** are adapted from REF.[40], Springer Nature Limited.
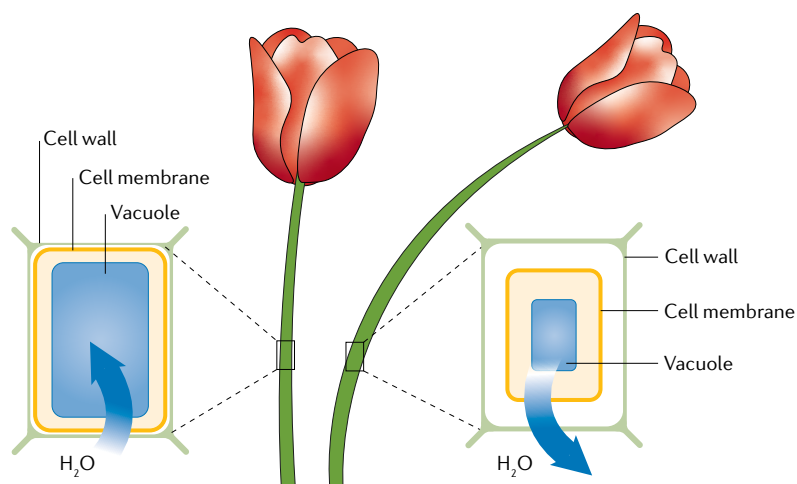
Fig. 5 | **Effect of hydration on turgor pressure in a plant stem.** An influx of water through the cell wall and into the vacuole causes it to swell and press against the cell membrane. This, in turn, expands the cell walls, rendering them more rigid and keeping the plant stem erect (namely, turgor pressure). The opposite effect — the efflux of water owing to dehydration —causes the cell walls to become flaccid and the plant wilts.

hinge absorbs water and the valves straighten and bend outwards, opening the capsule (FIG. 4b). This mechanism relies on the cellular structure and the active component in the inner side of the valve. The compact cellular tissue is arranged as a collapsed honeycomb under dry conditions (FIG. 4a). The highly swellable cellulose-filled cells are open-structured with porous lamellae between cellulosic mats. During hydration, the cellulose inner tissue absorbs water, causing the cells to expand into a honeycomb structure (FIG. 4c), which opens the valves of the seed capsule. We emphasize that, unlike the actuation systems discussed earlier (for example, pine cones, wheat awns and stork's bill awns), which are responsive to relative humidity changes, the responsive behaviour of ice plant seed capsules only occurs when they are exposed to liquid water. This behaviour arises because actuation is generated by the water uptake and swelling of the cellulose-filled cells. A pioneering investigation[73], which combined enthalpy-driven water adsorption and entropic gain of the system, demonstrated that this water–inner cellulose tissue interaction and the associated swelling are energetically sufficient to drive the full opening and closure of these seed capsules.

A similar mechanism exists in carrotwood seed pods. In contrast to the ice plant seed capsule, the seed pod of carrotwood opens upon dehydration and closes with increased humidity (FIG. 4d). The inner surface of each pod valve is covered by a fluffy fibrous layer acting as a cushion to provide protection for the seeds. The cross sections of a pod valve in their dry and wet states indicate that, beneath the fibrous cushion, there are two distinct layers comprising the valve tissue (FIG. 4d). The two optical microscopy images show different swelling potentials in each layer. As a consequence of the swelling caused by hydration, the thickness of the top layer of FIG. 4d (box labelled 'e' in FIG. 4d), corresponding to the inner layer of the pod, increases by about 300 μm, whereas the thickness of the bottom layer of FIG. 4d

(corresponding to the outside of the pod), which is sponge-like tissue, increases by approximately 500 μm (boxes labelled 'f' and 'g' in FIG. 4d). The swelling mismatch generates retraction of the pod valve, causing the closure of the seed pod upon hydration. This swelling mismatch is the result of the distinct structural features within these layers, and is revealed by the scanning electron microscopy images (FIG. 4e–g). The inner layer (top of FIG. 4d) is composed of fibres aligned along the thickness direction, whereas the outer layer (bottom of FIG. 4d) has a sponge-like porous structure with a pore-size gradient. There is a transitional region with a smaller pore size of ~10–20 μm (FIG. 4f), whereas the pore size in the outer layer is ~20–50 μm (FIG. 4g). The porous structure in the outer layer (FIG. 4g) exhibits a larger expansion upon hydration than the well-aligned fibres in the inner layer (FIG. 4e), producing anisotropic swelling in the pod valve tissue.

Turgor pressure from osmosis. Living turgid plant cells[74] contain a plasma membrane — a unique structure that is semipermeable and separates the cell organelles and cytoplasm from the external fluid. When a plant cell is immersed in a solution that has a different solute concentration from that within the cell, water passes through the semipermeable cell wall and plasma membrane to equilibrate the osmotic pressure between the outside and the inside of the cell, leading to a volumetric change (positive or negative, depending on whether water is flowing into or out of the cell, respectively). Plants wilt when water diffuses out through their walls and revive, becoming rigid as the concentration of water (and, thus, pressure) in the cells increases. The lipid bilayer that comprises the cell membrane is permeable to water but not to many other chemical substances. The cells in an erect stem are fully hydrated and expanded, whereas in the wilted state, water has diffused out of the cells, decreasing their volume (FIG. 5). The osmotic influx of water into the vacuole swells it and impinges on the cell membrane that pushes against the cell wall. By contrast, the efflux of water renders the cell flaccid. The equilibrium pressure inside the cell is called turgor pressure, and the cell is referred to as turgid when filled. An everyday example of this behaviour is flowers in a vase, which both wilt and regenerate as water flows out and into their cells. Cell swelling at the micrometre scale translates to increased stiffness at the structural (that is, macroscopic) level. In addition to the stiffness provided by turgid cells, there is an increase in the cross-sectional area, with an attendant increase in the moment of inertia.

Models of hydro-actuated deformation
The complex mechanochemistry of the effect of hydration on living and dead cells is not treated here, and the reader is referred to other sources[75–78]. In many passive systems, such as those discussed in previous sections, plants use a bilayer mechanism combined with anisotropic hygrometric expansion. In this section, we present two models based on a bilayer with a passive component, which, essentially, is unchanged, and an active component, which undergoes hygroscopically induced expansion. This expansion is often one-dimensional or

two-dimensional. These models account for the majority of hydration-induced deformation in plants.

A simple model was constructed incorporating these bilayer features for pine cone scales and wheat awns (FIG. 6a–d). A fibrous layer is considered, in which there is no increase in length in the longitudinal direction. This configuration corresponds to the alignment of the microfibrils being offset from that of the fibre cell axis by a small angle ($\mu < 45°$; FIG. 1b). For simplicity, these situations are represented by a layer consisting of parallel fibres. A hydration-sensitive layer is represented by the foundation (bottom layer), which corresponds to microfibrils forming a large angle ($\mu > 45°$) with the fibre axis. The reference system is defined in such a manner that the axis $0X_3$ is perpendicular to the surface. The swelling occurs along $0X_3$ (ε_{33}) and $0X_2$ (ε_{22}). The strain perpendicular to the interface does not contribute to distortion, such is the case for ε_{33}, which does not contribute to deformation. The angle of $0X_2$ with respect to the fibres in the fibrous layer determines the nature of deformation, such is the case for ε_{22}. If the angle is zero, bending takes place (FIG. 6a); if the angle
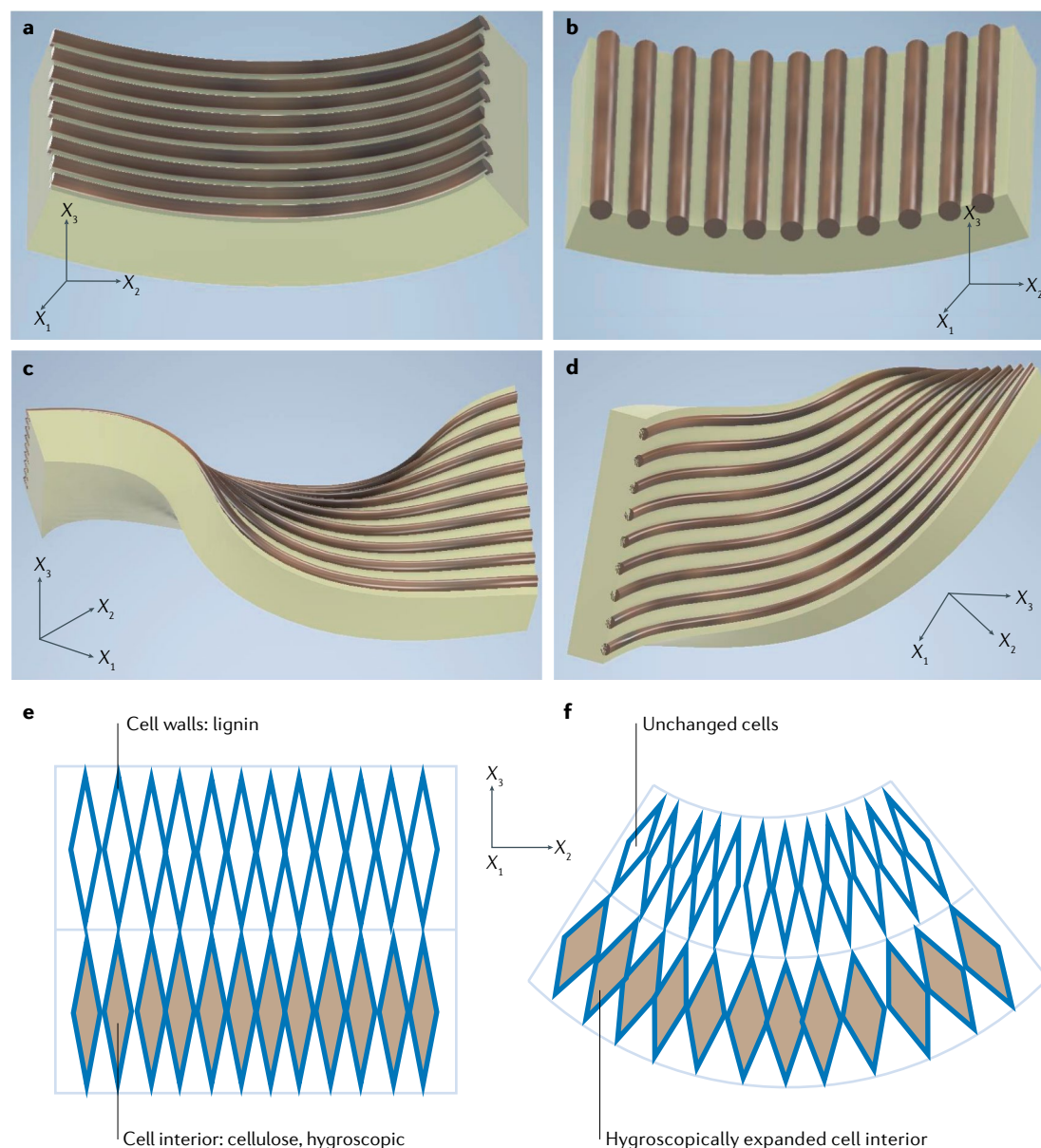

Fig. 6 | **Principal mechanisms operating in bilayer-based deformation of plants. a–d** | Simplified representations of hydration-induced deformation in wheat awns and pine cones. Two layers are assumed: a top layer consisting of fibres with fixed length (rods in the images) and a bottom layer consisting of a material that undergoes biaxial swelling with hydration. The strain ε_{11} is assumed to be zero (direction aligned with microfibrils, which do not change length), whereas strains ε_{22} and ε_{33} are non-zero and assume positive values upon hydration. **a** | Bending: $0X_2$ (ε_{22}) aligned with fibres. **b** | Saddling: $0X_2$ (ε_{22}) perpendicular to fibres. **c,d** | Helical twisting: $0X_2$ (ε_{22}) at +45° to the fibres for the positive helix and −45° to the fibres for the negative helix. **e,f** | Simplified representations of hydration-induced deformation in ice plant capsules: initial configuration with lignin cell walls (top) and hygroscopic cellulose-filled cells (bottom) (panel **e**); the cellulose inside the cells swells upon hydration and the volume increases, expanding the minor axis of the cells (panel **f**).

is 90°, warping or saddling occur (FIG. 6b); for +45°, a right-hand helix forms through twisting (FIG. 6c); and for −45°, a left-hand helix forms through twisting (FIG. 6d).

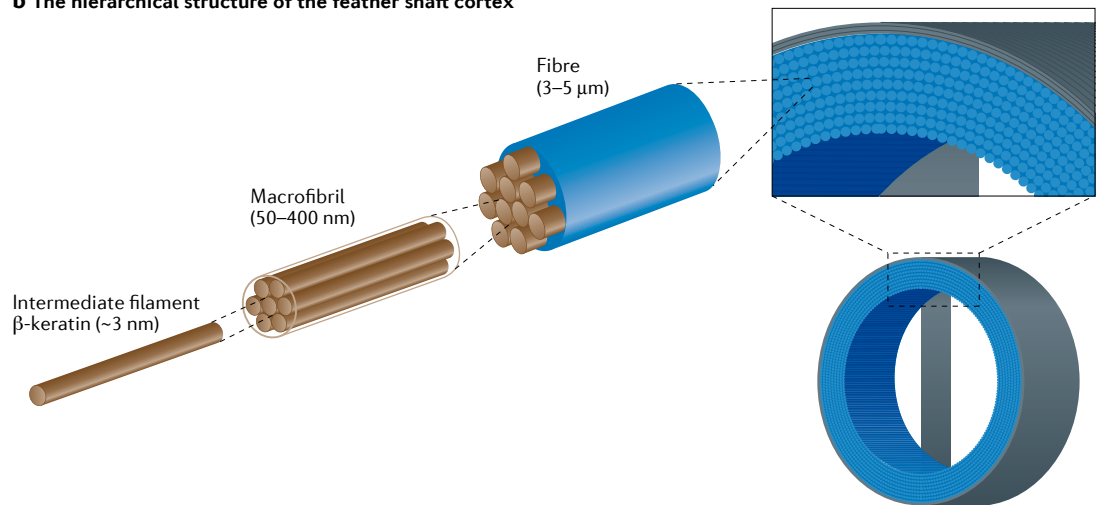The radii of curvature in bending and warping (or saddling) are readily calculated from the dimensions and coefficient of hygroscopic expansion, β (REF.[8]), which is defined in a similar manner to the thermal expansion coefficient:

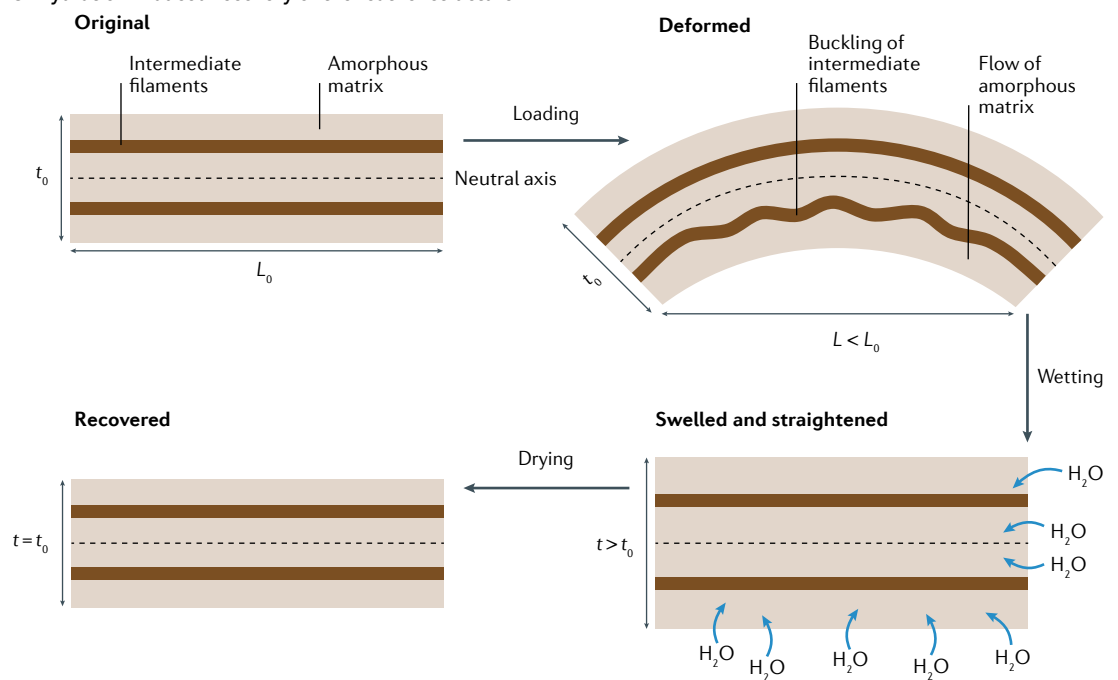$$\beta = \frac{\partial \varepsilon_{22}}{\partial \phi}$$

a The shape recovery of the shaft of a bird feather
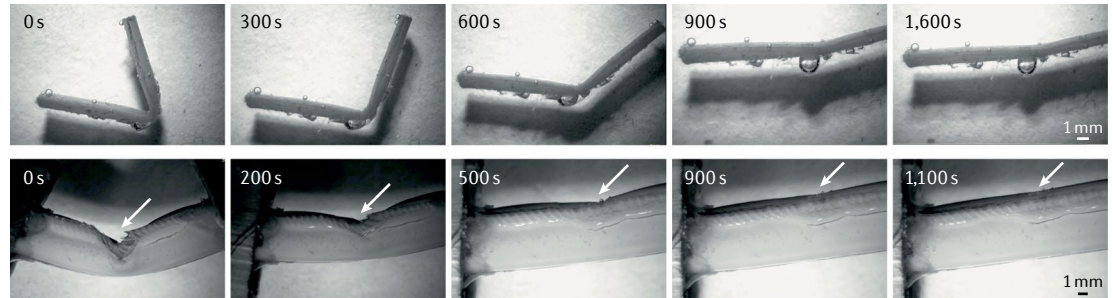
b The hierarchical structure of the feather shaft cortex

Fibre (3–5 μm)

Macrofibril (50–400 nm)

Intermediate filament β-keratin (~3 nm)

c Hydration-induced recovery of the feather structure

Original

Intermediate filaments

Amorphous matrix

t_0

Neutral axis

L_0

Loading

Deformed

Buckling of intermediate filaments

Flow of amorphous matrix

t_0

$L < L_0$

Wetting

Swelled and straightened

$t > t_0$

H_2O

H_2O

H_2O

H_2O H_2O H_2O H_2O H_2O

Recovered

$t = t_0$

Drying

This coefficient expresses the change in strain ε_{22} in the $0X_2$ direction with relative humidity, ϕ. Similarly, the pitch of the helix can be obtained by analysis.

The seed dispersal of ice plants is actuated through a similar mechanism (FIG. 6e,f). The top and bottom layers have a similar cell-wall structure. However, in the top layer, the lignified cells are empty, whereas the bottom cells are filled with a hygroscopic polysaccharide, which expands upon hydration. This expansion increases the minor axis of the rhombus-shaped cell walls and produces a positive strain, which is constrained by the top layer, thus, resulting in bending.

Recoverable materials in animals

Some extracellular matrix materials in animal tissues also manifest tunable properties with external triggers. For example, water is an integral component of collagen. Water removal from collagen shortens its molecular conformation, leading to significant contraction[79]. The resulting water-generated tensile stress has a role in collagenous tissues such as skin, tendon and bone. Another example is the jaws of *Nereis virens* — a species of marine worm — which are mainly composed of Nvjp-1 protein, yet, exhibit exceptional mechanical properties comparable to those of human dentin. It was recently discovered[80] that this jaw consists of condensed proteinaceous structures, the mechanical properties of which are tuned by coordination with transition-metal cations, particularly Zn^{2+}. This provides new inspiration for developing synthetic tunable materials. Other interesting tunable protein materials and their triggering mechanisms are being extensively investigated. In this section, we focus on the two most well-studied of these — keratin and spider silk — which have recoverable morphologies and mechanical properties that are dependent on the presence of water.

Keratinous materials

Keratin is a ubiquitous biological material, representing a group of impermeable filament- forming proteins with a high sulfur content. It is strong, tough and lightweight, and forms structural materials with many functions, such as armour (pangolin scales), weapons (nails, claws and horns), thermal insulator (hair and feathers) and transportation enabler (hooves and feathers)[81,82]. These keratinous structural materials are produced by specialized cells filled with keratin and are not associated with metabolism after they are formed; thus, these materials are usually considered as 'dead' tissue. Because keratinous materials are usually located at the most superficial layer on an animal's body, their intricate hierarchical structure confers them an excellent capability to recover their shape and strength by hydration, which significantly improves their durability. Typically, there are two phases: a crystalline phase, which is chemically crosslinked and provides a permanent structure for the material, and an amorphous phase, which consists of randomly organized molecular chains and branches that are interconnected with abundant hydrogen bonds, forming switches to enable tunable and temporary shape change. When the material is hydrated, the unbound water molecules enter the space between the polymer chains and branches, disrupting the original hydrogen bonds in the amorphous phase and making the material compliant for deformation. With an applied external force, the hydrated amorphous matrix flows, and the polymer chains and branches slide. During the dehydration process, unbound water evaporates, leaving the relocated chains and branches to form new hydrogen bonds between them, turning off the switch and fixing the material into a temporary shape. Once the material absorbs water again, the newly formed hydrogen bonds break again and, driven by entropic forces, the material recovers its original shape.

The precise mechanism remains unresolved. Notably, the reversible switching upon hydration and dehydration has been attributed to both hydrogen and disulfide bond breaking. Moreover, simple models assume a continuous crystalline phase, whereas others divide the crystalline phase into domains. In this section, we describe a simplified mechanism, in which the crystalline phase (intermediate filaments) is not affected by hydration, whereas the amorphous phase absorbs water and plasticizes. Thus, the intermediate filaments act as the passive component, in analogy with plants. The material can be 'trained' into a position upon drying by the formation of new hydrogen bonds in the amorphous phase. At the mesoscale, the interplay between crystalline and amorphous recovery (the latter developing reversible deformation) components determines the shape and strength (FIG. 7). This mechanism is similar to that in wood[59].

Here, we provide three examples of keratinous materials: bird feather, sheep horn and animal hair. Feathers are an evolutionary marvel that are not only lightweight but are also able to endure intense aerodynamic loads during flight, enabling aerial locomotion[83]. However, after flying for thousands of miles, fighting and other forms of environmental damage, structural deterioration is inevitable. In addition to preening, birds have developed a relaxing, yet, highly effective strategy to recover their damaged feathers: bathing. After severe plastic deformation, the feather can rapidly recover its original shape in less than 30 min with exposure to water (FIG. 7a). Preferential permeation of water into the amorphous phase allows hydrogen-bond breakage and subsequent swelling, which reorients and straightens the hierarchically arranged keratin fibrils and filaments (FIG. 7b), enabling recovery of the overall shape and mechanical properties[45] (FIG. 7c).

◀ Fig. 7 | **Hydration-induced shape and strength recovery of bird feathers. a |** The shape of a feather shaft (top), also shown at higher magnification (bottom) with the vane removed, is recovered in water after severe mechanical deformation. The arrows indicate the position of the deformation region and its gradual recovery, and the time after initial deformation is shown in seconds. **b |** The hierarchical structure of keratin fibres in bird feathers. **c |** A schematic representation of the mechanism for hydration-induced structural recovery in bird feathers. The original configuration has partially crystalline intermediate filaments with length L_0 embedded in an amorphous matrix, with thickness t_0. When an external load is applied, the deformation of the feather is enabled by the flow of the amorphous matrix and the buckling of the lower (below the neutral axis) intermediate filaments, decreasing the length to L ($L < L_0$). During the wetting process, water molecules penetrate the amorphous phase, causing the matrix to swell ($t > t_0$). Because the matrix is constrained by fibres, swelling stretches the buckled filaments and straightens the feather shaft. Finally, shrinking of the amorphous matrix by drying reverts the shape to its initial configuration. Panels **a** and **b** are reprinted with permission from REF.[45], Wiley.
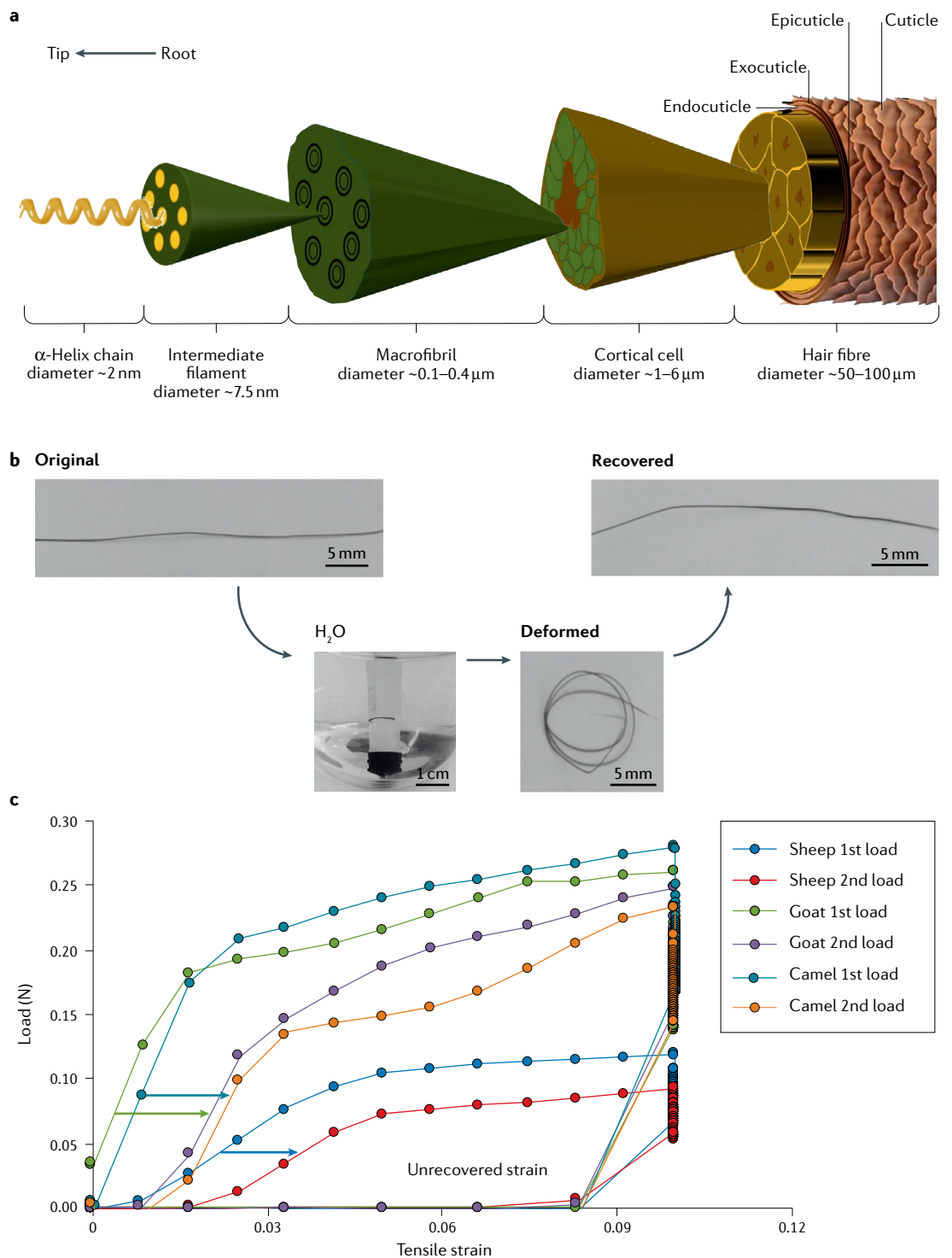
Fig. 8 | **Hydration-induced shape memory effect in animal hairs. a** | The hierarchical structure of (human) hair. The crystalline intermediate filaments are embedded in an amorphous matrix. **b** | The shape-recovery process induced by water for a camel hair. An originally straight hair is immersed in water and curls after being fully hydrated. The curled hair is dried to fix its temporary shape. After reimmersion in water, the curled hair returns to its original straight shape. **c** | Recovery of the mechanical strength of hairs from either sheep, goat or camel, after two loading cycles. Panel **a** is adapted with permission from REF.[85], Elsevier. Panels **b** and **c** are adapted from REF.[47], CC BY 4.0.

Horn is another common keratinous-based tool, which is possessed by many mammals, including cattle, goats, sheep, antelope and rhinoceroses. It serves as a powerful weapon to help these animals defend themselves from predators and fight members of their own species for territory, dominance or mating priority. As a highly effective energy-absorbent material[84], horn inevitably suffers damage during fighting, yet, can repair itself via hydration[46]. Unlike the well-aligned fibrous structure in feathers, horn is assembled by lamellae of keratinized

cells (Supplementary Fig. 3). However, similar to feathers, the building blocks of these keratin cells — the microfibrils — are composed of crystalline intermediate filaments that are embedded in an amorphous matrix. In horn, the recovery is much more limited because of the two-dimensional organization of the intermediate filaments and geometry. Fourier transform infrared spectroscopy provides evidence for preferential diffusion of

water to the amorphous phase through changes in C=O stretching and M–H bending with hydration[46]. New hydrogen bonds formed between water are evidenced by the decrease of free N–H bonds and eventual decrease of intensity. The intermediate filaments only underwent one-fifth of the strain (0.07) of the overall specimen in the hydrated tension state (failure at ~0.35). Although the compressive strength was recovered upon hydration,
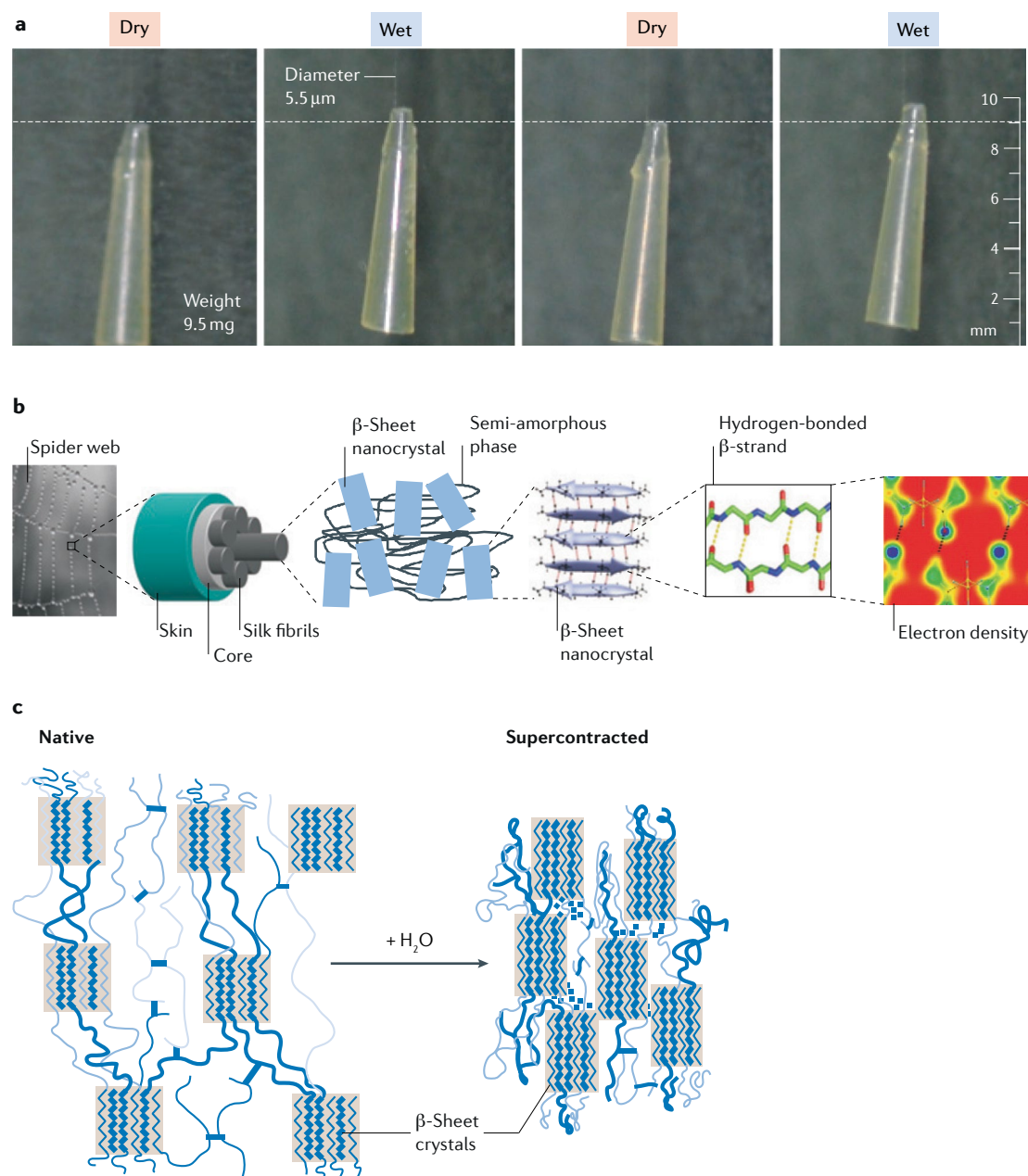

Fig. 9 | **Humidity-driven reversible supercontraction of spider silk as an artificial muscle. a** | Two cycles of humidity-driven, highly reversible contraction and relaxation for a spider silk thread subjected to a constant load from an applied weight. The dashed line indicates the displacement of the weight after one cycle of the silk contraction and relaxation. **b** | The hierarchical structure of spider silk. **c** | Structural model of native and supercontracted spider silk. The native spider silk has highly orientated β-sheet crystals interlinked by the glycine-rich chains, forming the crystalline and amorphous two-phase structure. In the amorphous phase, there is a Gaussian distribution of prestrains, which can be described by the worm-like chain model. As the humidity increases, the hydrogen bonds in the amorphous phase are broken by water molecules, releasing the prestrain and generating entropy-induced supercontraction. Panel **a** is reprinted with permission from REF.[88], The Company of Biologists. Panel **b** is reprinted from REF.[89], Springer Nature Limited. Panel **c** is adapted with permission from REF.[90], Royal Society of Chemistry.
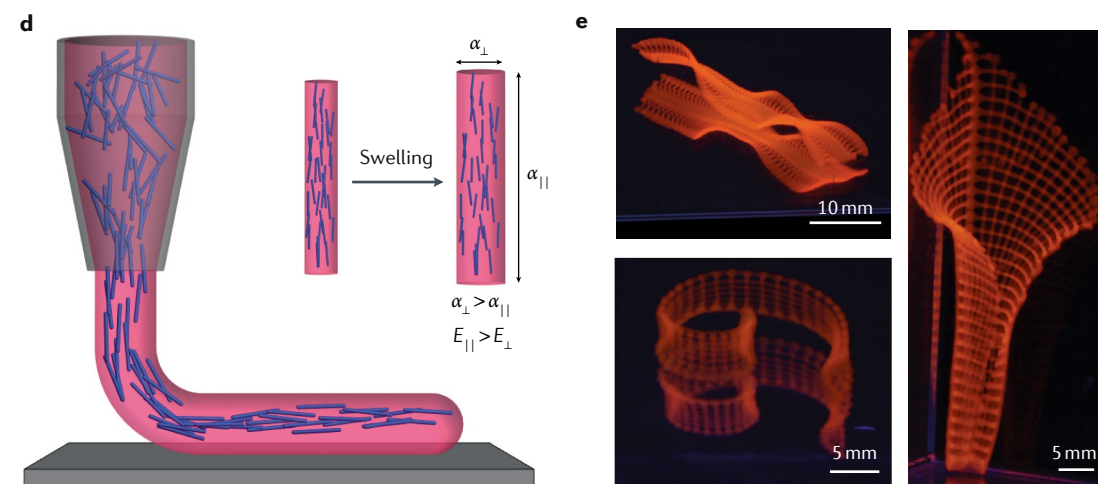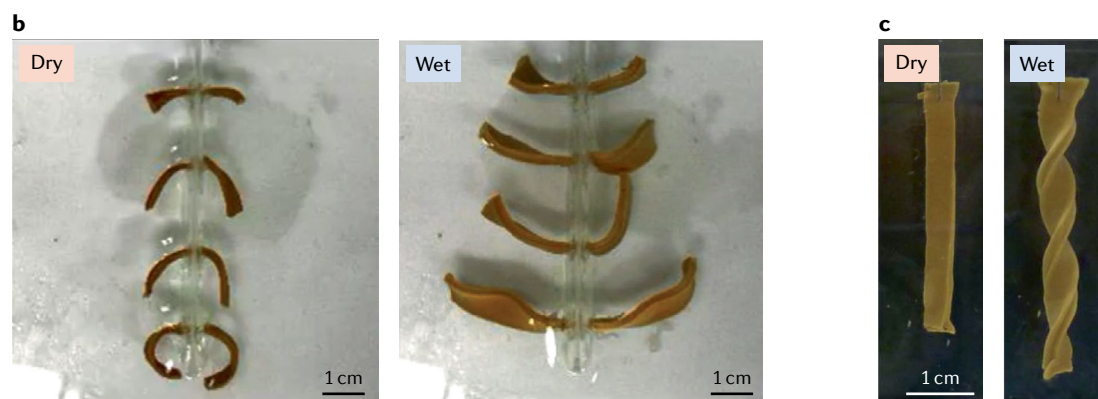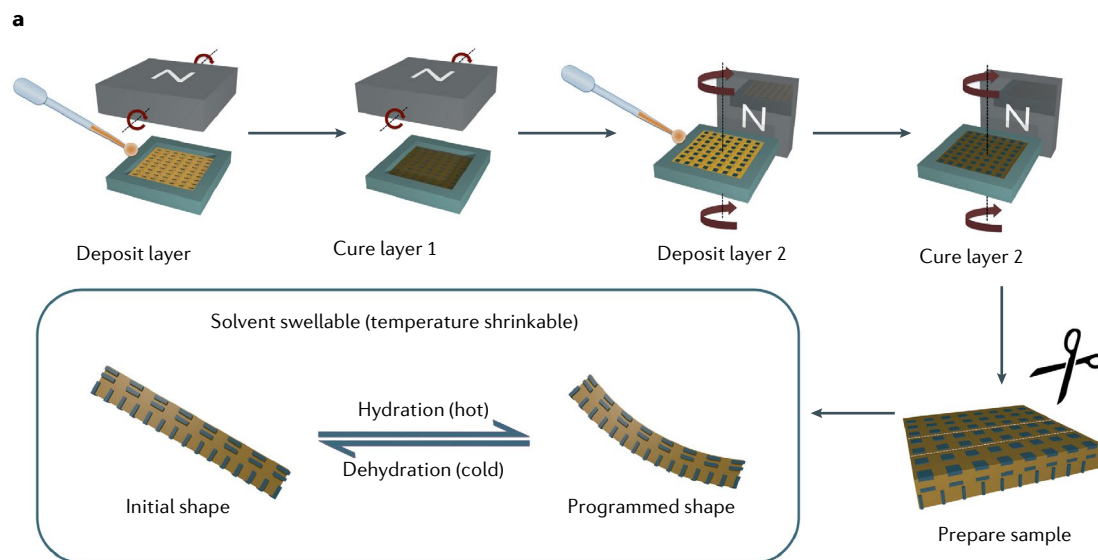
there was significant permanent damage in the form of plastic microbuckling, delamination and cracking.

A familiar, and everyday, recovery phenomenon of keratinous tissue is the hydration-induced shape recovery of hair. We all know that, no matter how messy our hair, a wash will enable recovery of the original form. The shape-recovery mechanism of hair is similar to that of other keratinous materials. The intricate structure of human hair contains hierarchical crystalline elements at different length scales (in ascending spatial scale: α-helices, intermediate filaments, macrofibrils and cortical cells) that are embedded in an amorphous matrix[85] (FIG. 8a). Most of the animal hair has similar structure, which also has two phases: filaments composed of crystalline elements with disulfide bonds between polypeptide chains and the matrix, which is composed of an

◄ Fig. 10 | **Bioinspired self-shaping materials manufactured by magnetic-field-controlled reinforcement and 4D printing. a** | Scheme of the magnetic-field-controlled manufacturing technique. Multilayered hydrogel matrix mixed with ultrahigh magnetic response alumina plates is fabricated in a Teflon mould under a weak magnetic field generated by a rotating permanent magnet. The ultrahigh magnetic response is produced by coating Al_2O_3 with iron-oxide nanoparticles and the orientation of this reinforcement in each layer is determined by the applied magnetic field. **b** | The hydro-actuated bending movement of the self-shaping hydrogel composites mimicking the reversible bending of pine cone scales. **c** | The hygroscopic twisting deformation mimicking the twisting opening of the *Bauhinia* pod. **d** | A schematic representation of a 4D printer nozzle and shear-induced one-step alignment of cellulose fibril reinforcement (blue) in a hydrogel matrix (pink) (left). The swelling strains, $\alpha_{\parallel}$ and $\alpha_{\perp}$, are shown, as well as the respective Young's moduli, $E_{\parallel}$ and $E_{\perp}$, denoted on the right. **e** | Hygroscopic deformations of twisting (top left) and curling (bottom left and right) generated by this 4D-printed hydrogel composite (a mirror is used to show different views of the material). Panels **a–c** are reprinted from REF.[17], Springer Nature Limited. Panels **d** and **e** are reprinted from REF.[97], Springer Nature Limited.

amorphous phase containing hydrogen bonds[47]. Upon deformation (and, often, the application of heat and hydration), hydrogen bonds in the amorphous phase are broken and reformed at different positions. Reversible hydration and dehydration processes turn on and off the switches, making geometrical and mechanical recovery possible[47] (FIG. 8b,c). For example, camel hair acquires this shape when formed into a circular shape and dried (FIG. 8b). Upon rehydration, the elastic energy stored in the crystalline phase restores the original shape, because the amorphous phase is 'softened' by water. Once dried, hair regains its original straight shape. FIGURE 8c shows that the mechanical strength of three types of animal hair (that is, sheep, goat and camel) is mostly recovered during two cyclic loading processes. This behaviour is at the foundation of the multi-billion-dollar haircare industry. There is an additional effect: a strain-induced α-to-β keratin transformation, which also contributes to the viscoelastic and plastic behaviour of hair[86,87], and increases the maximum strain. Whereas the elasticity from stretching of the chains is entropic, the conformational change from α-coils to β-sheets is driven by differences in internal energy[82].

Spider silk

Spider silks are extraordinary structural materials with strength and extensibility that are superior, by weight, to most human-made fibres. In addition, it has been proposed that spider dragline silk can undergo supercontraction induced by wetting, and that this has an important role in taking up slack in webs, restoring web shape and tension after prey capture, and opposing extensional forces exerted by the weight of precipitation (dew and rain) on webs[48]. The length change in a spider silk strand upon the cyclic variation of relative humidity (from 10% to 90%)[88] is highly reversible (FIG. 9a). Similar to keratin, spider silk is hierarchically constructed from crystalline domains embedded in an amorphous matrix. Each domain is assembled from the β-sheet nanocrystals of polyalanines connected within a semi-amorphous phase[89] (FIG. 9b). The crystalline phase has a permanent shape and the humidity-driven length tunability is conferred by the activation of the switch (that is, hydrogen bonds) in the amorphous phase[90] (FIG. 9c). The general idea is that the structure consists of crystals connected

with amorphous regions that act as 'springs' and shrink upon hydration. An added level of complexity is that the fibres are not homogeneous but are composed of a core and skin, in an analogous manner to hair[90]. This recoverable response provides inspiration for the design of novel actuators[48,49,88].

Bioinspired applications

Based on the design strategies identified in nature, many synthetic, hydration-induced, self-morphing materials have been successfully developed[17,91–103]. In this section, we provide four examples inspired by plant organs and two that mimic animal tissue discussed in the previous sections.

Inspired by the anisotropic swelling of plant organs directed by the cellulose microfibril angle in the cell wall, several types of programmable self-shaping material driven by humidity or thermal change have been fabricated. In one example, discontinuous, anisotropic alumina microplatelets were coated with superparamagnetic iron-oxide nanoparticles to render them magnetically responsive[17] (FIG. 10a). Based upon the ability to control the orientation of the platelets within different layers of a hydrogel composite using a weak external magnetic field, a multilayered swellable or shrinkable polymer matrix with stiff inorganic reinforcements oriented along different directions was fabricated. This structure mimics the structural design of self-shaping plant organs. By controlling the hydration or temperature, programmable passive movements, including bending (FIG. 10b) and twisting (FIG. 10c), were achieved.

Additive manufacturing, or 3D printing, is a powerful technique for creating composites with complex structures, including bioinspired structures. Recently, 4D printing has been developed, which extends 3D printing by incorporating the dimension of transformation over time. The 4D-printed materials can change to other structures upon the input of external energy, such as temperature, light or other environmental stimuli. With this technique, biomimetic hydrogel composites with bilayer structures programmed into various patterns have been developed. For example, a hydrogel composite reinforced with cellulose microfibrils[97] was constructed using this technique (FIG. 10d). In this case, the printing ink is aligned by the shear force acting on the filament during direct ink writing. The anisotropy of the stiffness and the swelling strain can be incorporated into the 4D-printing process by aligning the fibre (FIG. 10d). Using the same strategy as that identified in the movement of plant organs directed by cellulose microfibril angle, the printed hydrogel composites can localize swelling anisotropy and produce complex shape changes (such as bending, curling and twisting), once immersed in water (FIG. 10e).

Self-assembly is another effective synthetic method to produce complex structures through bottom-up processes, and is similar to the intricate pathways used for the formation of hierarchical structures in biological materials. Inspired by the morphogenesis in orchid petals (FIG. 11a), a self-shaping hydrogel by controlled molecular self-assembly was developed[98,99]. In this example, the morphology of a growing leaf was determined by
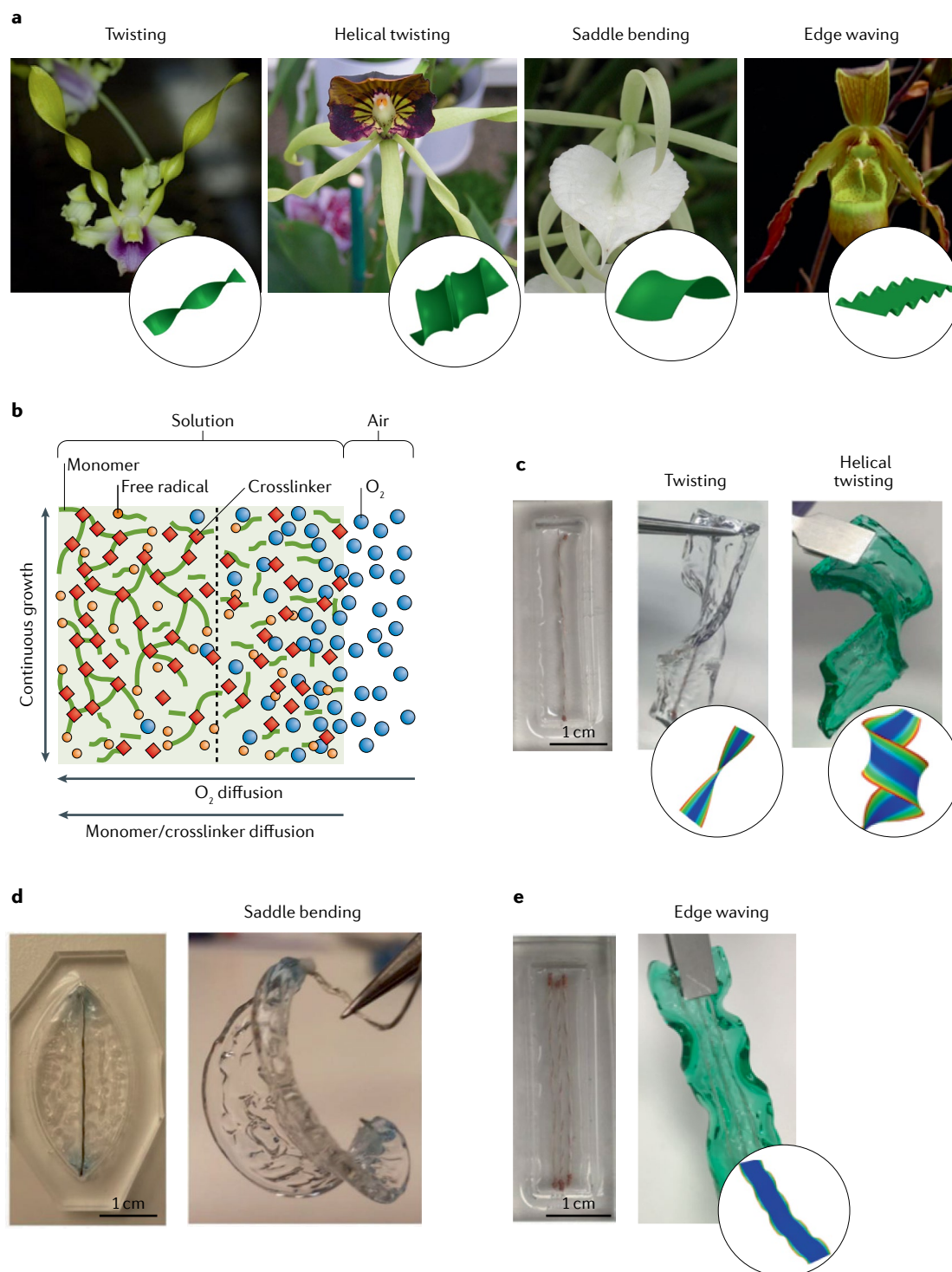
Fig. 11 | **Plant-inspired soft responsive materials fabricated by controlled molecular self- assembly. a** | Four types of differential growth and shape formation in plant organs: twisting (*Dendrobium helix*), helical twisting or coiling (*Prosthechea cochleata*), saddle bending (*Brassavola nodosa*) and edge waving (*Phragmipedium brasiliense*). The different morphologies of these leaves are determined by the maximum value and the spatial distribution of growth strains in the living leaf. **b** | Schematic representation of the self-assembly polymerization process induced by the diffusion of oxygen. The polymerization of hydrogels can be inhibited by the oxygen molecules. The gradient concentration of oxygen resulting from the diffusion, therefore, generates a gradient of gelation from the outer layer to the inner region. **c–e** | Anisotropic swelling conferred by gradient gelation in conjunction with an embedded stiff wire in the hydrogel matrix enables the hydrogels to achieve different responsive deformations, including twisting and helical twisting (panel **c**), saddle bending (panel **d**) and edge waving (panel **e**). The insets are simulation results from finite-element-analysis methods. Panels **a** (green insets), **c** and **e** are reprinted with permission from REF.[99], PNAS. Panel **a** twisting orchid image courtesy of P. Zorn. Panel **a** helical twisting orchid image reprinted from REF.[112], CC BY 3.0. Panel **a** saddle bending orchid image reprinted from REF.[113], CC BY 2.0. Panel **a** edge waving orchid image courtesy of Orchids Limited. Panels **b** and **d** are reprinted with permission from REF.[98], PNAS.

a Collagen–polyurethane artificial skin

Collagen triple helix

Soft segment
Hard segment

b Recovery process for artificial skin

Original
1 cm
→ Water →
Deformed
1 cm

↑ Dry

↓ Dry

10 min
1 cm

Fixed
1 cm

↑

↓ Water

60 s
1 cm

←

20 s
1 cm

c Silk acts as an artificial muscle

4.0 cm
Dry

3.5 cm
Wet

d Cyclic contraction (when wet) and expansion (when dry) of silk
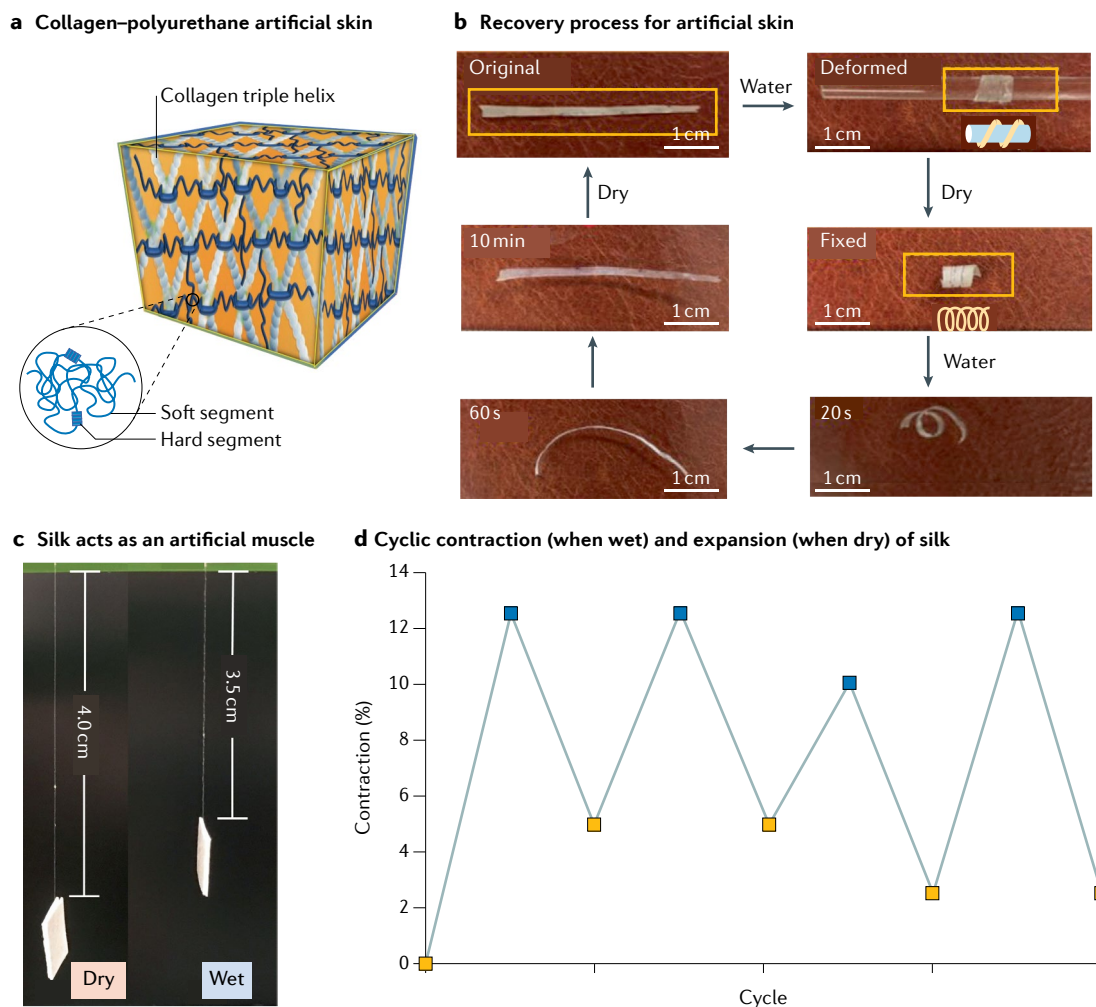
Contraction (%) vs Cycle

Fig. 12 | **Reversible hydration-induced motion in synthetic systems inspired by either skin or silk. a** | Artificial skin comprising a dual network of collagen–polyurethane has a water-responsive shape-memory effect. The artificial skin is fabricated from recycled calf skin and polyurethane solution. The reinforcing polyurethane has both soft segments and hard segments in the chain. **b** | A cycle of water-driven shape recovery for the biomimetic collagen–polyurethane composites. **c** | A representative humidity-driven supercontraction process showing that silk can act as an artificial muscle to lift weight (5 mg). **d** | Several cycles of weightlifting generated by the silk bundle. Panels **a** and **b** are adapted with permission from REF.[101], Royal Society of Chemistry. Panels **c** and **d** are reprinted with permission from REF.[102], CC BY 4.0.

both the maximum value and the spatial distribution of growth strain using a combination of experiments and simulations. Based on the parameters obtained from the plant organs, a hydrogel was fabricated using a graded polymerization process to replicate the morphogenesis processes in plant leaves. Owing to the inhibitive effect of oxygen on the polymerization of hydrogels, a graded gel (from the outer layer to the inner region) via controlled diffusion of air into the hydrogel solution (FIG. 11b) was generated. Embedded stiff wires in the soft hydrogels contributed to the anisotropic swelling strain (by constraining it along their orientation) and the composites achieved common leaf morphogenesis, such as twisting and helical twisting, saddle bending and edge waving (FIG. 11c–e, respectively).

These hydro-actuated self-shaping materials have not only been manufactured on a small scale but have already been used as biomimetic building skins on architectures sensitive to environmental changes at a large scale,

including a simple programmable veneer-composite system[100]. In this example, quarter-cut veneer of maple wood was further cut to make a semi-synthetic bilayer structure: a climate-responsive layer and a climate-independent layer. By manipulating the geometrical parameters, the programmable veneer can passively change its shape in response to humidity changes. This ingenious design has already been used as smart building skins to tune the permeability of architectures in response to change in humidity.

Several types of hydro-actuated shape-memory polymers have been inspired by animal tissues. Applying the dual-phase strategy that has been widely identified in shape-memory animal tissues, an artificial skin with a water-responsive shape-memory response was fabricated[101]. In this material, the major component of the mammal dermis was curvy collagen fibres, with some contribution from elastin (FIG. 12a). Waterborne polyurethane was impregnated into an entangled and

sticky collagen network, which was recycled from animal skin. The fabricated skin composite had two structural phases (FIG. 12a): type I collagen fibres and polyurethane chains composed of a soft and a hard segment. The interruption and regeneration of the hydrogen bonds within the collagen fibres act as the 'switch' to fix the temporary shape and recover the original geometry. One cycle of the shape-memory effect is possible in only 10 min, proving the success of shape-memory, biocompatible, synthetic polymers (FIG. 12b).

Spider silk is a popular source of natural inspiration, owing to its superb mechanical properties. Inspired by its reversible water-induced supercontraction, a smart fibre fabricated with a simple two-step synthesis achieved robust contraction through a hydration process and relaxed to its original conformation with dehydration[102]. In this example, fibres were drawn from a hydrogel composite and then treated with ultraviolet light at room temperature. The initial hydrogel was built from two components. Fibres drawn from the hydrogel have a double network: one formed from the physical interactions between the two components and the other from covalent crosslinks. As a consequence of this double-network structure, these synthetic fibres can work as a robust artificial muscle for lifting a weight of 5 mg (FIG. 12c), and can reversibly contract and relax for several cycles (FIG. 12d).

The application of the concept of osmotic deformation to synthetic devices is also an important area[103]. This mechanism operates within the plant cells and builds high internal pressures (up to 5 MPa), which lead to the stiffening of structures, as seen in hydrated plant stems (FIG. 5). This principle is used in soft robotics, in which the internal pressure increases the structural stiffness and deploys the device to the desired configuration.

Outlook

The intersection of additive manufacturing (4D printing), robotics and nanomotors is a fertile ground for the use of the concepts extracted from hydration-induced deformation. The tools provided by artificial intelligence and the Materials Genome Initiative will play a role in accelerating discovery. The form in which applications will take shape is difficult to predict because of the serendipity of discovery and the potential of novel functional behaviour. Until now, only proof-of-principle examples, which are extensions of observations in natural systems, have been demonstrated. Reaching the stage of technological utilization requires a focused and concerted developmental effort. For example, consider the gecko, which possesses reversible attachment devices on its paws. Although the scientific understanding of the effect has been known since the early 2000s[104–106], it took more than a decade to translate this understanding into applications[107]. Commercialization is now exploited in fields as diverse as robotics and biomedicine. This level of focused effort diverges significantly from academic research, which is exploratory, broad and directed at discovery and scientific inquiry. The developmental effort links the principles unravelled in fundamental research to an application and involves important technical work and the overcoming of bottlenecks.

In addition to the systems discussed in the last section, we provide indicators for new directions for technological implementation. For example, a bioinspired water-responsive polymer composite consisting of two polymers was used to generate power through a piezoelectric actuator[108]. The maximum stress generated (upon dehydrating) was 27 MPa. This actuation force is a very high value and approaches the strength of some polymers. The 0.3-Hz response is orders of magnitude higher than the response of natural systems, where hydration takes tens of minutes and dehydration about twice as long. This superb performance suggests a manner in which reversible bioinspired hydration can be used to drive nanomotors and nanorobots without any external source of energy. The cyclic time, τ, is related to the diffusion distance, h, through $\tau \sim \frac{h^2}{D}$ (where D is the diffusion coefficient of water in the medium); thus, the smaller h, the greater the achievable frequency. Thus, nanorobots are especially suited to be driven by this process because of their small dimensions, which reduce the cycle time[109].

Techniques such as 4D printing can be game changers because they enable the fabrication of spatially varying compositions and resulting graded behaviour. 4D printing has been used to create synthetic pine cone scales[110]. The two layers are a polymer not particularly affected by moisture and a mixture of polymer and wood fibres; the latter become aligned with the filamentary-deposition process in such a manner that they exhibit a prescribed swelling upon hydration. 4D printing has also been used to produce composite hydrogels that have localized, anisotropic swelling behaviour controlled by the alignment of cellulose fibrils along predefined 4D-printing pathways. This methodology enabled the fabrication of plant-inspired architectures that change shape upon immersion in water, and is another example of how these technologies can bridge the gap between biological materials and their bioinspired analogues.

Although our understanding of the biological structures responsible for reversible hydro-actuated deformation has rapidly expanded, there are aspects that are poorly understood. For instance, there are reports of bilayer structures with porosity and elastic-modulus gradients that can decrease interfacial stresses; these structures have important roles in biological structures. The optimum gradients should be analytically predicted, which can provide insight into why the reversible deformation of, for instance, cone scales can be conducted for a large number of cycles without fatigue failure owing to internal stresses, a performance still not matched by synthetic designs[111].

There is a connection, albeit still in its infancy, between morphogenesis (the phenomenon by which different organs grow in biological systems) and hygromorphs. Morphogenesis in plant leaves yields helical twisting, twisting and saddle bending. The resulting shapes are similar to those produced by hydro-actuation[99]. The elasticity-based morphogenesis framework can be extended to hydro-actuation (for example, in flowers).

The design principle of the ice plant seed capsule has been modelled analytically and by the finite element method[40,73]. These studies demonstrated that

significant strains (up to 3) can be obtained by expanding a rhombus-shaped structure using internal pressure. Moreover, it was shown that the filling of the honeycomb structure by a hygroscopic material can produce internal reversible expansion. Nevertheless, the detailed nature of the processes involved is only partially understood.

The differential uptake of water in the amorphous and crystalline phases of plant and animal tissue is not sufficiently understood. The answer is likely embedded in a more detailed understanding of the chemistry and finer, nanoscale features of the amorphous and crystalline phases. Specifically, it is crucial to explain why the crystalline part is resistant to water uptake. For instance, water can penetrate into the less crystallized hemicellulose matrix in plant cells and the cortex matrix in keratin, while the more crystallized cellulose and intermediate filaments are less permeable. In addition, our understanding does not explain the thermodynamics or kinetics of the water uptake or the diffusion rate of water in these two phases. A deeper understanding will enable the rate of change of configurations and potential for translation to engineered mimics.

Inspired by the ingenious designs found in nature, smart synthetic materials, such as self-shaping composites, as well as some robust artificial muscles, have been developed at different length scales. Now, it is necessary to apply the lessons from nature to develop responsive materials with simpler simulative strategies and better biocompatibility to fulfil the requirements of modern manufacturing industries based on intelligent devices.

Published online: 05 November 2020

1. Zhang, X. et al. The pathway to intelligence: using stimuli-responsive materials as building blocks for constructing smart and functional systems. *Adv. Mater.* **31**, 1804540 (2019).
2. Sokolov, I. L., Cherkasov, V. R., Tregubov, A. A., Buiucli, S. R. & Nikitin, M. P. Smart materials on the way to theranostic nanorobots: molecular machines and nanomotors, advanced biosensors, and intelligent vehicles for drug delivery. *Biochim. Biophys. Acta, Gen. Subj.* **1861**, 1530–1544 (2017).
3. Holdren, J. P. et al. Materials Genome Initiative Strategic Plan. Technical Report December 2014. *National Science and Technology Council* https://www.mgi.gov/sites/default/files/documents/mgi_strategic_plan_-_dec_2014.pdf (2014).
4. Raccuglia, P. et al. Machine-learning-assisted materials discovery using failed experiments. *Nature* **533**, 73–73 (2016).
5. Qin, Z. et al. Artificial intelligence method to design and fold alpha-helical structural proteins from the primary amino acid sequence. *Extreme Mech. Lett.* **36**, 100652 (2020).
6. Yu, C. H., Qin, Z. & Buehler, M. J. Artificial intelligence design algorithm for nanocomposites optimized for shear crack resistance. *Nano Futures* **3**, 035001 (2019).
7. Yang, C. Q., Wu, Z. S. & Ye, L. P. Self-diagnosis of hybrid CFRP rods and as-strengthened concrete structures. *J. Intell. Mater. Syst. Struct.* **17**, 609–618 (2006).
8. Inada, H., Okuhara, Y. & Kumagai, H. in *Sensing Issues in Civil Structural Health Monitoring* (ed. Ansari F.) 239–248 (Springer, 2005).
9. Fukui, Y., Fukuda, M. & Fujimoto, K. Generation of mucin gel particles with self-degradable and -releasable properties. *J. Mater. Chem. B* **6**, 781–788 (2018).
10. Nakajima, N., Sugai, H., Tsutsumi, S. & Hyon, S. H. Self-degradable bioadhesive. *Key Eng. Mater.* **342–343**, 713–716 (2007).
11. Hager, M. D., Greil, P., Leyens, C., van der Zwaag, S. & Schubert, U. S. Self-healing materials. *Adv. Mater.* **22**, 5424–5430 (2010).
12. Wu, D. Y., Meure, S. & Solomon, D. Self-healing polymeric materials: a review of recent developments. *Prog. Polym. Sci.* **33**, 479–522 (2008).
13. Speck, O. & Speck, T. An overview of bioinspired and biomimetic self-repairing materials. *Biomimetics* **4**, 26 (2019).
14. Asquith, R. S., Blair, H. S., Crangle, A. A. & Riordan, E. Self-colored polymers based on anthraquinone residues. *J. Soc. Dye. Colour.* **93**, 114–125 (1977).
15. Wang, Z. et al. A novel mechanochromic and photochromic polymer film: when rhodamine joins polyurethane. *Adv. Mater.* **27**, 6469–6474 (2015).
16. Oliver, K., Seddon, A. & Trask, R. S. Morphing in nature and beyond: a review of natural and synthetic shape-changing materials and mechanisms. *J. Mater. Sci.* **51**, 10663–10689 (2016).
17. Erb, R. M., Sander, J. S., Grisch, R. & Studart, A. R. Self-shaping composites with programmable bioinspired microstructures. *Nat. Commun.* **4**, 1712 (2013).
18. Gibson, J. S. et al. Reconfigurable antennas based on self-morphing liquid crystalline elastomers. *IEEE Access* **4**, 2340–2348 (2016).

19. Otsuka, K. & Ren, X. Physical metallurgy of Ti-Ni-based shape memory alloys. *Prog. Mater. Sci.* **50**, 511–678 (2005).
20. Hager, M. D., Bode, S., Weber, C. & Schubert, U. S. Shape memory polymers: past, present and future developments. *Prog. Polym. Sci.* **49–50**, 3–33 (2015).
21. Lai, A., Du, Z. H., Gan, C. L. & Schuh, C. A. Shape memory and superelastic ceramics at small scales. *Science* **341**, 1505–1508 (2013).
22. Leng, J. S., Lan, X., Liu, Y. J. & Du, S. Y. Shape-memory polymers and their composites: stimulus methods and applications. *Prog. Mater. Sci.* **56**, 1077–1135 (2011).
23. Wang, Z., Li, K., He, Q. & Cai, S. A light-powered ultralight tensegrity robot with high deformability and load capacity. *Adv. Mater.* **31**, 1806849 (2019).
24. He, Q., Wang, Z., Song, Z. & Cai, S. Bioinspired design of vascular artificial muscle. *Adv. Mater. Technol.* **4**, 1800244 (2019).
25. Pikul, J. H. et al. Stretchable surfaces with programmable 3D texture morphing for synthetic camouflaging skins. *Science* **358**, 210–214 (2017).
26. Geetha, M., Singh, A. K., Asokamani, R. & Gogia, A. K. Ti based biomaterials, the ultimate choice for orthopaedic implants–a review. *Prog. Mater. Sci.* **54**, 397–425 (2009).
27. Lendlein, A. & Langer, R. Biodegradable, elastic shape-memory polymers for potential biomedical applications. *Science* **296**, 1673–1676 (2002).
28. Stuart, M. A. et al. Emerging applications of stimuli-responsive polymer materials. *Nat. Mater.* **9**, 101–113 (2010).
29. Langer, R. & Tirrell, D. A. Designing materials for biology and medicine. *Nature* **428**, 487–492 (2004).
30. Meyers, M. A., McKittrick, J. & Chen, P. Y. Structural biological materials: critical mechanics-materials connections. *Science* **339**, 773–779 (2013).
31. Fratzl, P. & Weinkamer, R. Nature's hierarchical materials. *Prog. Mater. Sci.* **52**, 1263–1334 (2007).
32. Ritchie, R. O. The conflicts between strength and toughness. *Nat. Mater.* **10**, 817–822 (2011).
33. Teyssier, J., Saenko, S. V., van der Marel, D. & Milinkovitch, M. C. Photonic crystals cause active colour change in chameleons. *Nat. Commun.* **6**, 6368 (2015).
34. DeMartini, D. G., Krogstad, D. V. & Morse, D. E. Membrane invaginations facilitate reversible water flux driving tunable iridescence in a dynamic biophotonic system. *Proc. Natl Acad. Sci. USA* **110**, 2552–2556 (2013).
35. Szulgit, G. K. & Shadwick, R. E. Dynamic mechanical characterization of a mutable collagenous tissue: response of sea cucumber dermis to cell lysis and dermal extracts. *J. Exp. Biol.* **203**, 1539–1550 (2000).
36. Thurmond, F. & Trotter, J. Morphology and biomechanics of the microfibrillar network of sea cucumber dermis. *J. Exp. Biol.* **199**, 1817–1828 (1996).
37. Allen, R. D. Mechanism of the seismonastic reaction in *Mimosa pudica*. *Plant Physiol.* **44**, 1101–1107 (1969).
38. Stuhlman, O. & Darden, E. B. The action potentials obtained from Venus's-flytrap. *Science* **111**, 491–492 (1950).

39. Dawson, C., Vincent, J. F. V. & Rocca, A. M. How pine cones open. *Nature* **390**, 668 (1997).
40. Harrington, M. J. et al. Origami-like unfolding of hydro-actuated ice plant seed capsules. *Nat. Commun.* **2**, 337 (2011).
41. Armon, S., Efrati, E., Kupferman, R. & Sharon, E. Geometry and mechanics in the opening of chiral seed pods. *Science* **333**, 1726–1730 (2011).
42. Elbaum, R., Zaltzman, L., Burgert, I. & Fratzl, P. The role of wheat awns in the seed dispersal unit. *Science* **316**, 884–886 (2007).
43. Abraham, Y. et al. Tilted cellulose arrangement as a novel mechanism for hygroscopic coiling in the stork's bill awn. *J. R. Soc. Interface* **9**, 640–647 (2012).
44. Liu, Z. Q., Jiao, D. & Zhang, Z. F. Remarkable shape memory effect of a natural biopolymer in aqueous environment. *Biomaterials* **65**, 13–21 (2015).
45. Sullivan, T. N., Zhang, Y. L., Zavattieri, P. D. & Meyers, M. A. Hydration-induced shape and strength recovery of the feather. *Adv. Funct. Mater.* **28**, 1801250 (2018).
46. Huang, W. et al. How water can affect keratin: hydration-driven recovery of bighorn sheep (*Ovis canadensis*) horns. *Adv. Funct. Mater.* **29**, 1901077 (2019).
47. Xiao, X. L. & Hu, J. L. Animal hairs as water-stimulated shape memory materials: mechanism and structural networks in molecular assemblies. *Sci. Rep.* **6**, 26393 (2016).
48. Liu, Y., Shao, Z. & Vollrath, F. Relationships between supercontraction and mechanical properties of spider silk. *Nat. Mater.* **4**, 901–905 (2005).
49. Liu, D. et al. Spider dragline silk as torsional actuator driven by humidity. *Sci. Adv.* **5**, eaau9183 (2019).
50. Skotheim, J. M. & Mahadevan, L. Physical limits and design principles for plant and fungal movements. *Science* **308**, 1308–1310 (2005).
51. Forterre, Y., Skotheim, J. M., Dumais, J. & Mahadevan, L. How the Venus flytrap snaps. *Nature* **433**, 421–425 (2005).
52. Hofhuis, H. & Hay, A. Explosive seed dispersal. *New Phytol.* **216**, 339–342 (2017).
53. Llorens, C. et al. The fern cavitation catapult: mechanism and design principles. *J. R. Soc. Interface* **13**, 20150930 (2016).
54. Evangelista, D., Hotton, S. & Dumais, J. The mechanics of explosive dispersal and self-burial in the seeds of the filaree, *Erodium cicutarium* (Geraniaceae). *J. Exp. Biol.* **214**, 521–529 (2011).
55. Deegan, R. D. Finessing the fracture energy barrier in ballistic seed dispersal. *Proc. Natl Acad. Sci. USA* **109**, 5166–5169 (2018).
56. Witztum, A. & Schulgasser, K. The mechanics of seed expulsion in Acanthaceae. *J. Theor. Biol.* **176**, 531–542 (1995).
57. Rafsanjani, A., Brulé, V., Western, T. L. & Pasini, D. Hydro-responsive curling of the resurrection plant *Selaginella lepidophylla*. *Sci. Rep.* **5**, 8064 (2015).
58. Elbaum, R. & Abraham, Y. Insights into the microstructures of hygroscopic movement in plant seed dispersal. *Plant Sci.* **223**, 124–133 (2014).
59. Fratzl, P., Elbaum, R. & Burgert, I. Cellulose fibrils direct plant organ movements. *Faraday Discuss.* **139**, 275–282 (2008).
60. Barthelat, F., Yin, Z. & Buehler, M. J. Structure and mechanics of interfaces in biological materials. *Nat. Rev. Mater.* **1**, 16007 (2016).

REVIEWS

61. Evert, R. F. & Eichhorn, S. E. Raven biology of plants, 8th edn. Reviewed by Chaffey, N. *Ann. Bot.* **113**, vii (2014).
62. Wei, L. & McDonald, A. G. A review on grafting of biofibers for biocomposites. *Materials* **9**, 303 (2016).
63. Elbaum, R., Gorb, S. & Fratzl, P. Structures in the cell wall that enable hygroscopic movement of wheat awns. *J. Struct. Biol.* **164**, 101–107 (2008).
64. Goswami, L. et al. Stress generation in the tension wood of poplar is based on the lateral swelling power of the G-layer. *Plant J.* **56**, 531–538 (2008).
65. Timoshenko, S. Analysis of bi-metal thermostats. *J. Opt. Soc. Am.* **11**, 233–255 (1925).
66. Harlow, W. M., Côté, W. A. & Day, A. C. The opening mechanism of pine cone scales. *J. For.* **62**, 538–540 (1964).
67. Poppinga, S. et al. Hygroscopic motions of fossil conifer cones. *Sci. Rep.* **7**, 40302 (2017).
68. Reyssat, E. & Mahadevan, L. Hygromorphs: from pine cones to biomimetic bilayers. *J. R. Soc. Interface* **6**, 951–957 (2009).
69. Elbaum R. in *Plant Biomechanics: From Structure to Function at Multiple Scales* (eds Geitmann, A. & Gril, J.) 235–246 (Springer, 2018).
70. Fahn, A. & Zohary, M. On the pericarpial structure of the legumen, its evolution and relation to dehiscence. *Phytomorphology* **5**, 99–111 (1955).
71. Rascio, N. & Rocca, N. L. Resurrection plants: the puzzle of surviving extreme vegetative desiccation. *Crit. Rev. Plant Sci.* **24**, 209–225 (2005).
72. Shen, J. H., Xie, Y. M., Zhou, S. W., Huang, X. D. & Ruan, D. Water-responsive rapid recovery of natural cellular material. *J. Mech. Behav. Biomed. Mater.* **34**, 283–293 (2014).
73. Razghandi, K. et al. Hydro-actuation of ice plant seed capsules powered by water uptake. *Bioinspired Biomim. Nanobiomater.* **3**, 169–182 (2014).
74. Steudle, E., Zimmermann, U. & Lüttge, U. Effect of turgor pressure and cell size on the wall elasticity of plant cells. *Plant Physiol.* **59**, 285–289 (1977).
75. Burgert, I. & Fratzl, P. Actuation systems in plants as prototypes for bioinspired devices. *Philos. Trans. R. Soc. A* **367**, 1541–1557 (2009).
76. Braam, J. In touch: plant responses to mechanical stimuli. *New Phytol.* **165**, 373–389 (2005).
77. Egan, P., Sinko, R., LeDuc, P. R. & Keten, S. The role of mechanics in biological and bio-inspired systems. *Nat. Commun.* **6**, 7418 (2015).
78. Lachenbruch, B. & McCulloh, K. A. Traits, properties, and performance: how woody plants combine hydraulic and mechanical functions in a cell, tissue, or whole plant. *New Phytol.* **204**, 747–764 (2014).
79. Masic, A. et al. Osmotic pressure induced tensile forces in tendon collagen. *Nat. Commun.* **6**, 5942 (2015).
80. Chou, C. C. et al. Ion effect and metal-coordinated cross-linking for multiscale design of *Nereis* jaw inspired mechanomutable materials. *ACS Nano* **11**, 1858–1868 (2017).
81. Wang, B., Yang, W., McKittrick, J. & Meyers, M. A. Keratin: structure, mechanical properties, occurrence in biological organisms, and efforts at bioinspiration. *Prog. Mater. Sci.* **76**, 229–318 (2016).
82. McKittrick, J. et al. The structure, functions, and mechanical properties of keratin. *JOM* **64**, 449–468 (2012).
83. Wang, B. & Meyers, M. A. Light like a feather: a fibrous natural composite with a shape changing from round to square. *Adv. Sci.* **4**, 1600360 (2017).
84. Huang, W., Zaheri, A., Jung, J. Y., Espinosa, H. D. & McKittrick, J. Hierarchical structure and compressive deformation mechanisms of bighorn sheep (*Ovis canadensis*) horn. *Acta Biomater.* **64**, 1–14 (2017).
85. Yu, Y., Yang, W., Wang, B. & Meyers, M. A. Structure and mechanical behavior of human hair. *Mater. Sci. Eng. C* **73**, 152–163 (2017).
86. Yu, Y., Yang, W. & Meyers, M. A. Viscoelastic properties of α-keratin fibers in hair. *Acta Biomater.* **64**, 15–28 (2017).
87. Miserez, A. & Guerette, P. A. Phase transition-induced elasticity of α-helical bioelastomeric fibres and networks. *Chem. Soc. Rev.* **42**, 1973–1995 (2012).
88. Agnarsson, I., Dhinojwala, A., Sahni, V. & Blackledge, T. A. Spider silk as a novel high performance biomimetic muscle driven by humidity. *J. Exp. Biol.* **212**, 1989–1993 (2009).
89. Keten, S., Xu, Z., Ihle, B. & Buehler, M. J. Nanoconfinement controls stiffness, strength and mechanical toughness of β-sheet crystals in silk. *Nat. Mater.* **9**, 359–367 (2010).
90. Ene, R., Papadopoulos, P. & Kremer, F. Combined structural model of spider dragline silk. *Soft Matter* **5**, 4568–4574 (2009).
91. Montero de Espinosa, L., Meesorn, W., Moatsou, D. & Weder, C. Bioinspired polymer systems with stimuli-responsive mechanical properties. *Chem. Rev.* **117**, 12851–12892 (2017).
92. Song, K. & Lee, S. J. Pine cone scale-inspired motile origami. *NPG Asia Mater.* **9**, e389 (2017).
93. de Haan, L. T., Verjans, J. M. N., Broer, D. J., Bastiaansen, C. W. M. & Schenning, A. P. H. J. Humidity-responsive liquid crystalline polymer actuators with an asymmetry in the molecular trigger that bend, fold and curl. *J. Am. Chem. Soc.* **136**, 10585–10588 (2014).
94. Ionov, L. Biomimetic hydrogel-based actuating systems. *Adv. Funct. Mater.* **23**, 4555–4570 (2013).
95. Zhao, Q. et al. An instant multi-responsive porous polymer actuator driven by solvent molecule sorption. *Nat. Commun.* **5**, 4293 (2014).
96. Guiducci, L., Fratzl, P., Brechet, Y. & Dunlop, J. W. Pressurized honeycombs as soft-actuators: a theoretical study. *J. R. Soc. Interface* **11**, 20140458 (2014).
97. Sydney Gladman, A., Matsumoto, E. A., Nuzzo, R. G., Mahadevan, L. & Lewis, J. A. Biomimetic 4D printing. *Nat. Mater.* **15**, 413–418 (2016).
98. Huang, C., Quinn, D., Suresh, S. & Hsia, K. J. Controlled molecular self-assembly of complex three-dimensional structures in soft materials. *Proc. Natl Acad. Sci. USA* **115**, 70–74 (2018).
99. Huang, C., Wang, Z., Quinn, D., Suresh, S. & Hsia, K. J. Differential growth and shape formation in plant organs. *Proc. Natl Acad. Sci. USA* **115**, 12359–12364 (2018).
100. Reichert, S., Menges, A. & Correa, D. Meteorosensitive architecture: biomimetic building skins based on materially embedded and hygroscopically enabled responsiveness. *Comput. Aided Des.* **60**, 50–69 (2015).
101. Han, Y., Hu, J. & Chen, X. A skin inspired bio-smart composite with water responsive shape memory ability. *Mater. Chem. Front.* **3**, 1128–1138 (2019).
102. Wu, Y. et al. Biomimetic supramolecular fibers exhibit water-induced supercontraction. *Adv. Mater.* **30**, 1707169 (2018).
103. Stahlberg, R. The phytomimetic potential of three types of hydration motors that drive nastic plant movements. *Mech. Mater.* **41**, 1162–1171 (2009).
104. Autumn, K. et al. Adhesive force of a single gecko foot-hair. *Nature* **405**, 681–685 (2000).
105. Autumn, K. et al. Evidence for van der Waals adhesion in gecko setae. *Proc. Natl Acad. Sci. USA* **99**, 12252–12256 (2002).
106. Arzt, E., Gorb, S. & Spolenak, R. From micro to nano contacts in biological attachment devices. *Proc. Natl Acad. Sci. USA* **100**, 10603–10606 (2003).
107. Hensel, R., Moh, K. & Arzt, E. Engineering micro-patterned dry adhesives: from contact theory to handling applications. *Adv. Funct. Mater.* **28**, 1800865 (2018).
108. Ma, M., Guo, L., Anderson, D. G. & Langer, R. Bio-inspired polymer composite actuator and generator driven by water gradients. *Science* **11**, 186–189 (2013).
109. Shin, B. et al. Hygrobot: A self-locomotive ratcheted actuator powered by environmental humidity. *Sci. Robot.* **3**, eaar2629 (2018).
110. Correa, D. et al. 4D pine scale: biomimetic 4D printed autonomous scale and flap structures capable of multi-phase movement. *Phil. Trans. R. Soc. A* **378**, 20190445 (2019).
111. Liu, Z., Meyers, M. A., Zhang, Z. & Ritchie, R. O. Functional gradients and heterogeneities in biological materials: design principles, functions, and bioinspired applications. *Prog. Mater. Sci.* **88**, 467–498 (2017).
112. Higgins, W. E. *Prosthechea chochleata. Kew Science* http://powo.science.kew.org/taxon/urn:lsid:ipni.org:names:1001247-1#sources (2017).
113. Wikimedia Commons. *Brassavola nodosa. Wikimedia Commons* https://commons.wikimedia.org/wiki/File:Brassavola_nodosa_-_Flicker_003.jpg (2017).

Author Contributions
H.Q. wrote the first draft of the paper and developed the figures. D.K. provided advice in bioinspired applications. M.A.M. conceived the structure and focus of this paper and participated actively in the writing and illustrations.

Competing interests
The authors declare no competing interests.

Publisher's note
Springer Nature remains neutral with regard to jurisdictional claims in published maps and institutional affiliations.

Supplementary information
Supplementary information is available for this paper at https://doi.org/10.1038/s41578-020-00251-2.

RELATED LINKS
Orchids Limited: https://www.orchidweb.com/orchids/phragmipedium/species/phrag-brasiliense-clone-a